

Hypergraph Neural Network with State Space Models for Node Classification

A. Quadir^a, M. Tanveer^{a,*}

^a*Department of Mathematics, Indian Institute of Technology Indore, Simrol, Indore, 453552, Madhya Pradesh, India*

Abstract

In recent years, graph neural networks (GNNs) have gained significant attention for node classification tasks on graph-structured data. However, traditional GNNs primarily focus on adjacency relationships between nodes, often overlooking the role-based characteristics that can provide complementary insights for learning expressive node representations. Existing frameworks for extracting role-based features are largely unsupervised and often fail to translate effectively into downstream predictive tasks. To address these limitations, we propose a hypergraph neural network with a state space model (HGMN). The model integrates role-aware representations into GNNs by combining hypergraph construction with state-space modeling in a principled manner. HGMN employs hypergraph construction techniques to capture higher-order relationships and leverages a learnable mamba transformer mechanism to fuse role-based and adjacency-based embeddings. By exploring two distinct hypergraph construction strategies, degree-based and neighborhood-based, the framework reinforces connectivity among nodes with structural similarity, thereby enriching the learned representations. Furthermore, the inclusion of hypergraph convolution layers enables the model to account for complex dependencies within hypergraph structures. To alleviate the over-smoothing problem encountered in deeper networks, we incorporate residual connections, which improve stability and promote effective feature propagation across layers. Comprehensive experiments on benchmark datasets including OGB, ACM, DBLP, IIP TerroristRel, Cora, Citeseer, and Pubmed demonstrate that HGMN consistently outperforms strong baselines in node classification tasks. These results support the claim that explicitly incorporating role-based features within a hypergraph framework offers tangible benefits for node classification tasks.

Keywords: Graph neural networks, Hypergraph, State space model, Node classification.

^{*}Corresponding author

Email addresses: `mscphd2207141002@iiti.ac.in` (A. Quadir), `mtanveer@iiti.ac.in` (M. Tanveer)

1. Introduction

Graph-based modeling has become a powerful paradigm for analyzing complex relational data, with applications spanning social networks [1], molecular interactions [2], and brain connectivity [3]. Graph neural networks (GNNs) extend traditional neural architectures by leveraging graph structure, achieving strong performance across diverse tasks [4]. Representative models such as GCN [5], GAT [6], and GraphSAGE [7] exemplify this progress. These frameworks operate under the message-passing framework [8], where node representations are iteratively updated by aggregating features from their neighbors. This design effectively captures local structural dependencies and enhances both node- and graph-level representations. In real-world graphs, nodes often represent distinct roles or functions, yet nodes with similar roles are not always directly connected. Traditional GNNs such as GCN [5], GAT [6], and GraphSAGE [7] generate embeddings by aggregating information from immediate neighbors. Jumping knowledge networks (JK-Nets) [9] aggregate information across GNN layers to adaptively capture neighborhood features at different depths. While effective for capturing local structures, this framework has two major limitations: (1) it struggles to produce role-specific representations that capture fine-grained semantic or structural functions, and (2) it fails to connect role-similar nodes that are distant or lack direct edges. A node’s role may reflect semantic attributes (e.g., student, advisor, manager) or structural properties within the network (e.g., opinion leader, bridge, structural hole spanner) [10]. Although unsupervised role representation frameworks [11, 12] have been proposed, their effectiveness in downstream tasks remains limited. Moreover, adjacency-based multi-layer GNNs are prone to over-smoothing, where node embeddings become indistinguishable after repeated message passing. Traditional GNNs mainly operate on standard graphs that capture pairwise node adjacencies, often neglecting the role-based relationships that exist among nodes. In contrast, hypergraphs [13] can be constructed from conventional graphs in various ways, enabling the modeling of higher-order interactions. By encoding richer connections among nodes and clusters, hypergraph adjacency facilitates more expressive aggregation, allowing graph neural networks to effectively integrate both role-based and adjacency-driven representations.

Recently, graph transformers have emerged as powerful models for capturing long-range interactions between nodes [14, 15]. Unlike traditional message-passing frameworks that emphasize local edge-level neighborhoods [5, 16], attention mechanisms in graph transformers enable each node to attend to all others, offering a global perspective on graph structure [17]. To further advance this paradigm, the GraphGPS framework combines structural and positional encodings (SE/PE), a message-passing neural network (MPNN), and an attention module. Together, these components enrich node and edge embeddings and improve performance on downstream tasks. Its modular design also supports the seamless integration of diverse

attention mechanisms, providing flexibility and adaptability for different applications [18]. Graphomer [19] adapts transformers to graphs, capturing long-range dependencies, but standard transformers often underperform on graph-specific tasks due to limited structural awareness. GROVER [20] addresses this with self-supervised pretraining on large-scale molecular graphs, learning richer node and motif representations. GraphMAE [21] leverages masked graph autoencoding to capture both local and global patterns efficiently.

The quadratic computational cost of the attention mechanism restricts the scalability of transformers for long sequences, despite their strong modeling capacity. Moreover, fully attending to all tokens is not always necessary or optimal, as long-range dependencies may not require exhaustive contextual encoding. Empirical evidence indicates that simply increasing context length often fails to yield consistent improvements in sequence model performance [22]. State space models (SSMs) have emerged as a promising alternative to attention-based architectures [23], offering greater efficiency for long sequences. However, their effectiveness is limited by time-invariant transition mechanisms, which constrain their ability to perform input-dependent context compression. Recently, Mamba has demonstrated remarkable success in language modeling, surpassing transformers of the same size and achieving performance on par with models that are twice as large. These advancements have motivated growing interest in extending Mamba’s architecture to diverse data modalities [24, 25].

Building on the concept of hypergraphs [13], we propose the hypergraph neural network with a state space model (HGMN). This framework is designed to integrate both adjacency-based and role-based representations into graph learning. Unlike conventional GNNs that primarily rely on local message passing, HGMN employs two complementary hypergraph construction strategies based on node degree and neighborhood levels. These strategies capture higher-order relationships and reinforce connections among nodes with similar roles, even when they are distant in the original graph. To effectively unify these heterogeneous perspectives, HGMN incorporates a Mamba-inspired state space mechanism with adaptive weighting. The mechanism enables a flexible balance between structural and role-driven features. Hypergraph convolution layers are further utilized to jointly learn adjacency and role-based dependencies, while residual connections mitigate over-smoothing and enhance stability during training. Collectively, these design choices make HGMN a robust and versatile model, capable of producing richer and more discriminative node representations than standard GNNs. As a result, graph learning tasks that require the integration of both structural connectivity and role-aware semantics are significantly enhanced.

The paper’s key highlights are as follows:

1. We propose a novel hypergraph neural network with state space model (HGMN), which integrates role-based representations into graph neural networks. HGMN leverages hypergraph construction

techniques to effectively combine adjacency and role-based node representations from higher-order perspectives.

2. Two unique hypergraph construction methods are incorporated, based on node degree and neighborhood levels. These methods enhance role representation learning by ensuring stronger connections between nodes with similar roles in the hypergraph structure.
3. HGMN incorporates a learnable mamba transformer mechanism to efficiently merge role-based and adjacency-based node representations, enabling adaptive and robust representation learning.
4. By employing hypergraph convolution layers, HGMN learns hypergraph structures during training. To address the over-smoothing problem common in graph neural networks, a residual network is incorporated, improving the stability and expressiveness of the model.
5. Compared to traditional GNNs, HGMN provides enriched node representations by embedding role characteristics and utilizing a more effective aggregation strategy. This makes the model versatile and applicable to a wide range of node representation tasks involving adjacency structures and role information.
6. HGMN effectiveness is validated through comprehensive experiments on four publicly available datasets. The results demonstrate that HGMN achieves significant performance gains, with absolute improvements of up to 12.1% in node classification accuracy compared to existing GNN frameworks.

Table 1: List of symbols and their definitions used in HGMN.

Symbols	Definition and description
G	A general undirected graph
E_l, E_d	Hyperedge by node link, and node degree
X_r, X_a	Role embeddings, and adjacency embeddings
G_h^l, G_h^d	Hypergraphs constructed by node link, and node degree
D_v^l, D_v^d	Node degree matrices by node link, and node degree
D_e^l, D_e^d	Hyperedge degree matrices by node link, and node degree
Y	The label of nodes
J	The embedding of nodes

2. Preliminaries and related work

An undirected graph can be represented as $G = (V, E, A)$, where $V = \{v_1, v_2, \dots, v_N\}$ is the set of nodes, $A \in \mathbb{R}^{N \times N}$ is the adjacency matrix, and E represents the set of edges. The role representation is denoted as $X_r \in \mathbb{R}^{N \times F_r}$, $X_a \in \mathbb{R}^{N \times F_a}$ corresponds to the adjacency-based representation, and $X_f \in \mathbb{R}^{N \times F_h}$ denotes the fused embedding. Node labels are indicated by $Y \in \mathbb{R}^N$, where the nodes belong to M distinct categories. GNNs generate the node representations $J \in \mathbb{R}^{N \times F_h}$ and use them to predict the labels of the nodes. For

hypergraph construction, the incidence matrix is denoted as H , with D_v and D_e representing the node degree and hyperedge degree matrices, respectively. Model training involves learnable parameters δ , and the coefficients λ , α , and β are used for regularization and feature fusion. Table 1 lists the notations used in the HGNN model.

2.1. Graph Neural Network

Graph Neural Networks (GNNs), first introduced by Scarselli et al. [26], are designed to analyze graph-structured data and have achieved success in diverse domains such as knowledge representation [27], text generation [28], traffic prediction [29], and weather forecasting [30]. Early spectral frameworks, including ChebNet [31] and its simplification GCN [5], pioneered localized feature propagation. Later frameworks, such as UniMP [32] and SAT [15], further extended adjacency-based message passing by incorporating label propagation or subgraph representations.

To enrich graph representations beyond adjacency, models such as ID-GNN [33] and PGNN [34] integrated node identity and positional encodings, while GLOGNN and GLOGNN++ [35] introduced co-efficient matrices to capture higher-order correlations. Other directions explored multiscale and spectral perspectives, for example, SAGNN [36] models cross-scale interactions, and GWNN [37] leverages wavelet transforms to address limitations of Fourier-based methods. Recent progress in graph representation learning has demonstrated broad applicability across domains such as fraud detection, multi-agent dynamics, fault diagnosis, and intelligent resource management [38]. The H2IDE model [39] addresses homophily–heterophily challenges in multi-relational graphs using disentangled representation learning and relation-aware attention for effective fraud detection. Extending structural modeling, Shi et al. [40] employed hypergraphs and a Fokker–Planck framework to capture higher-order interactions in multi-agent systems. Interpretability has also gained prominence, with Wang et al. [41] introducing a causal graph, a guided GNN for interpretable fault diagnosis in nuclear systems. Similarly, the dynamic parking model [42] leverages neural prediction and control for adaptive resource allocation.

2.2. Hypergraph Learning

Hypergraph learning was first proposed as a framework for propagating information over hypergraph structures, where degree-free hyperedges enable modeling of high-order correlations beyond simple pairwise relationships [43]. Building on this foundation, Feng et al. [13] and Yadati et al. [44] pioneered the integration of hypergraph structures into GNNs, laying the groundwork for subsequent advancements. For example, Bai et al. [45] introduced hypergraph attention networks and hypergraph convolutional neural networks to strengthen representation learning, while Zhang et al. [46] developed the dual-channel hypergraph

convolutional framework (DHCf) to improve collaborative filtering in recommendation systems. Further generalizations have been proposed, such as Chien et al. [47], who introduced a framework that dynamically selects propagation methods according to dataset characteristics, and Yang et al. [48], who designed an attention-based hypergraph neural network to prioritize informative features. Collectively, these works establish hypergraph neural networks as powerful tools for capturing complex, higher-order dependencies across domains. However, their potential for explicitly modeling role-based node representations, which are crucial for tasks where adjacency alone is insufficient, remains largely unexplored.

2.3. State Space Models

State space models (SSMs) form a broad family of sequence modeling frameworks, ranging from classical hidden Markov models to recurrent neural networks (RNNs) in modern deep learning. These models maintain context by recurrently updating hidden states, integrating new inputs with past information to generate outputs. While effective for sequential data, traditional SSMs often face challenges in scalability and efficiency. To address these limitations, structured state space models (S4) introduced reparameterization techniques that significantly improve computational efficiency, offering a streamlined alternative to the quadratic cost of attention mechanisms [49].

Building on S4, a wave of linear-time attention models has been proposed, including hungry hungry hippos (H3) [50], Hyena [51], and receptance weighted key value (RWKV) [52], all designed to capture long-range dependencies while maintaining efficiency. Extending this line of work, Mamba introduces a data-driven selection mechanism within S4, enabling adaptive context compression as sequence lengths grow [22]. This design achieves linear-time complexity while outperforming Transformers of comparable or larger sizes across diverse long-sequence benchmarks. Moreover, Mamba’s adaptability has been demonstrated beyond sequential domains, including computer vision tasks such as image segmentation, where its ability to capture long-range contextual information leads to substantial performance gains [53].

3. Hypergraph Neural Network with State Space Model (HGMN)

The proposed HGMN framework captures both role-based and adjacency-based node features while modeling long-range dependencies by integrating hypergraph representation learning with state-space models. To illustrate the overall workflow, Fig. 1 outlines four main stages: first, role and adjacency features are extracted from the input graph using Node2vec [13] and Graphwave [12]; next, hypergraphs are constructed to encode higher-order relationships among nodes; these features are then adaptively fused using a Mamba-based structured state-space model (SSM) attention mechanism; finally, the fused representations are propagated through hypergraph convolutional layers, enhanced via residual learning, and fed into

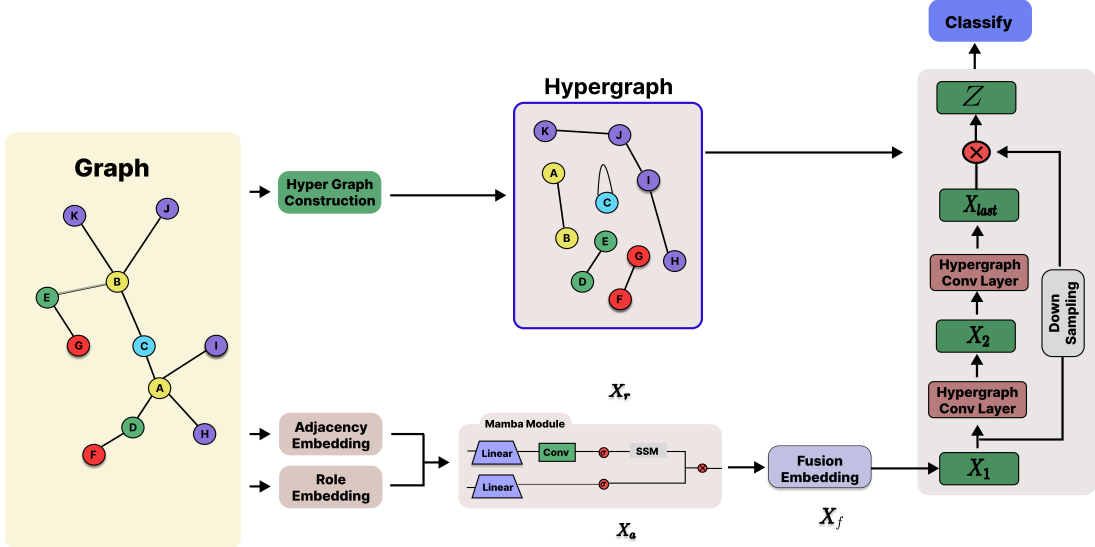


Figure 1: Overview of the proposed HG-MN. The input graph is first converted into a hypergraph to capture higher-order node relationships. Node features are transformed into adjacency-based (X_a) and role-based (X_r) embeddings, which are fused via the Mamba module using linear projections, convolution, and a state-space model, producing X_f . Fused embeddings pass through hierarchical hypergraph convolution layers with downsampling to generate multi-level representations (X_1, \dots, X_{last}), which are aggregated and fed to a classifier for node-level prediction.

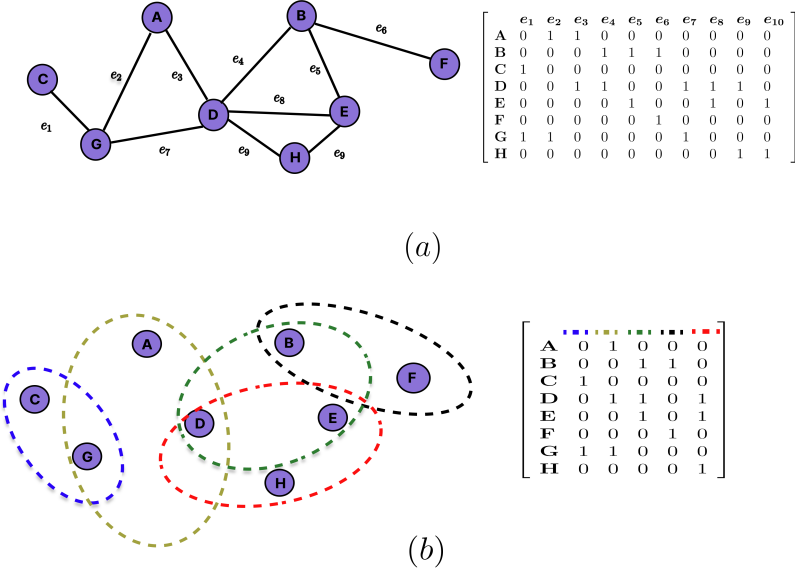


Figure 2: Simple Graph vs. Hypergraph. (a) A traditional graph with edges connecting pairs of nodes and its vertex-edge incidence matrix. (b) A hypergraph where hyperedges can connect multiple nodes simultaneously, with the corresponding incidence matrix. Hypergraphs capture higher-order relationships that simple graphs cannot, motivating the proposed HG-MN to model complex node interactions for improved representation learning.

the classification module. This staged design ensures that HG-MN effectively integrates local, global, and higher-order structural information for robust graph representation learning.

3.1. Construction of Hypergraph

To extend traditional pairwise graphs into higher-order structures, HGMN relies on hypergraph construction. Unlike a standard graph, where an edge connects only two nodes, a hypergraph allows a hyperedge to connect multiple nodes that share common characteristics, thereby capturing richer relationships among them. Formally, a hypergraph is defined as $G_H = (V_H, E_H, W_H)$, where V_H denotes the set of nodes, E_H the set of hyperedges, and W_H the hyperedge weight matrix. The incidence relation is described by $\theta(v, e) \in \{0, 1\}$, which indicates whether node v belongs to hyperedge e . Based on this definition, the degree of a hyperedge and node is given by:

$$d(e_i) = \sum_{v_i \in V} \theta(v_i, e_i), \quad (1)$$

$$d(v_i) = \sum_{e_i \in E} \theta(v_i, e_i) w(e_i), \quad (2)$$

with the corresponding degree matrices for nodes and hyperedges denoted by D_v and D_e . These formulations establish the mathematical foundation for constructing hypergraphs within HGMN, as illustrated in Fig. 2.

To capture different structural perspectives, we employ two complementary strategies for constructing hypergraphs:

3.1.1. Node-Link Hypergraph

The first approach leverages the local neighborhood of each node in the input graph G . Specifically, the neighbors of a central node are grouped together to form a hyperedge, producing the hypergraph G_h^l . The resulting incidence matrix is represented as $H^l \in \mathbb{R}^{N \times N_E^l}$, where N is the number of nodes in G and N_E^l the number of generated hyperedges. The associated degree matrices are denoted by D_v^l and D_e^l . This construction emphasizes local connectivity by clustering nodes based on shared adjacency relations.

3.1.2. Degree-Based Hypergraph

The second approach groups nodes according to their degree values. Nodes with identical degrees form a common hyperedge, creating the hypergraph G_h^d . The structure is encoded by the incidence matrix $H^d \in \mathbb{R}^{N \times N_E^d}$, where N_E^d corresponds to the number of distinct node degrees in the graph. The degree matrices of this hypergraph are denoted as D_v^d and D_e^d . This method highlights global structural roles by linking nodes with similar connectivity levels.

Together, these two construction methods enable HGMN to capture both local adjacency-based relationships and global role-based similarities, providing a richer foundation for subsequent feature aggregation.

tion in the hypergraph convolutional network. Once hypergraphs capture both local and global structural information, we employ the Mamba state-space model to fuse role-based and adjacency-based features while efficiently modeling long-range dependencies.

3.2. Mamba Workflow

A central challenge in graph representation learning is the effective integration of local adjacency-based information and global role-based features. Standard attention mechanisms, while powerful, are computationally expensive for large graphs and may not fully capture long-range dependencies. To address this, HGMN incorporates the Mamba state space model (SSM) [22], which provides a linear-time alternative to traditional attention while maintaining strong capability in modeling long sequences. This makes Mamba well-suited for handling the dynamic interactions between structural and role-based embeddings. Fig. 3 illustrates the integration of adjacency-based and role-based features through the Mamba transformer mechanism, where structured state-space layers with learnable parameters adaptively fuse the two representations into a unified embedding.

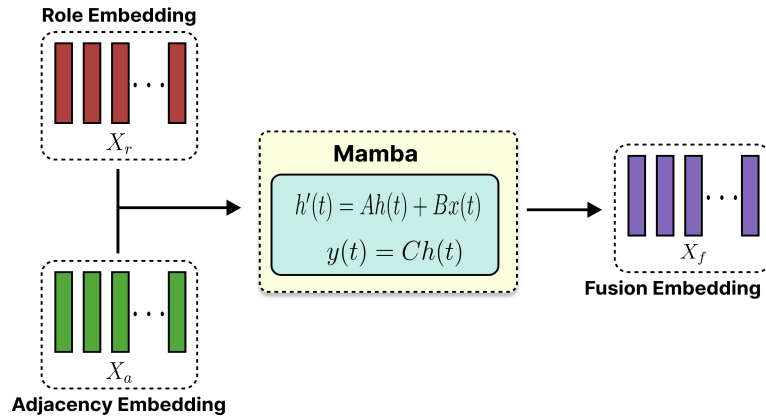


Figure 3: Illustration of the Mamba transformer mechanism within HGMN. The block takes adjacency-based features (\hat{X}_a) and role-based features (\hat{X}_r) as inputs, processes them through structured state-space layers with learnable parameters (A, B, C), and adaptively fuses the resulting outputs using attention coefficients (\hat{v}_a, \hat{v}_r). The fused embedding X_f captures both structural and role-aware information, making the mechanism well-suited for integrating higher-order graph dependencies.

Formally, an SSM models sequential dependencies through a latent state that evolves according to a linear ordinary differential equation (ODE). For an input sequence $x(t) \in \mathbb{R}^N$, the hidden state $h(t)$ and output sequence $y(t)$ are defined as:

$$\begin{aligned} h'(t) &= Ah(t) + Bx(t), \\ y(t) &= Ch(t), \end{aligned} \tag{3}$$

where $A \in \mathbb{R}^{N \times N}$ is the state matrix, and $B, C \in \mathbb{R}^N$ are input and output matrices. Since solving this ODE directly is intractable, it is discretized for practical use:

$$h_t = \bar{A}h_{t-1} + \bar{B}x_t, \quad y_t = Ch_t, \quad (4)$$

where the parameters \bar{A} and \bar{B} are derived from A, B , and the step size Δ .

Within HGMN, the SSM adaptively fuses role-based and adjacency-based embeddings. The SSM acts as a lightweight yet expressive attention mechanism, learning how information should be propagated across different roles and structural contexts in the hypergraph. Specifically, the fusion is realized through attention coefficients applied to role and adjacency embeddings:

$$X_f = \hat{y}_r \hat{X}_r + \hat{y}_a \hat{X}_a. \quad (5)$$

where \hat{X}_r and \hat{X}_a are the role-based and adjacency-based embeddings, and \hat{y}_r, \hat{y}_a are the learned attention weights from the SSM. The fused embedding $X_f \in \mathbb{R}^{N \times F_h}$ then serves as the input to the hypergraph convolutional layers. With the fused embeddings from Mamba, the hypergraph convolution layer aggregates higher-order features to encode both local adjacency and global role-based interactions.

3.3. Hypergraph Convolution Layer

The fused embedding X_f , which the Mamba-based attention mechanism produces (Eq. (5)), serves as the input to the hypergraph convolutional network. Unlike standard GNN pipelines that rely solely on adjacency information, this design ensures that both role-based dependencies and structural connectivity patterns are jointly encoded before propagation. The hypergraph convolution layer then performs higher-order feature aggregation as follows:

$$X^{(l)} = \sigma \left(D_v^{-1} H W_H D_e^{-1} H^T D_v^{-1} X^{(l-1)} \delta^{(l-1)} \right) \quad (6)$$

where H is the incidence matrix that encodes node–hyperedge relations, and D_v, D_e are the degree matrices of nodes and hyperedges used for normalization. The weight matrix W_H captures how information flows across hyperedges, while the learnable parameter $\delta^{(l-1)}$ adaptively modulates contributions from neighboring nodes. Finally, the nonlinearity σ introduces expressive power by enabling the network to learn complex interactions.

Integrating Mamba before the convolution step allows the model to capture long-range and role-aware dependencies that traditional hypergraph convolutions alone cannot efficiently represent. The convolution

layer then grounds these enriched features in the hypergraph structure, ensuring that role–adjacency interactions are propagated across higher-order neighborhoods. This two-stage design, Mamba-based fusion followed by hypergraph convolution, enables HGNN to balance global context modeling with structural consistency, ultimately leading to more accurate and robust graph representation learning. To further stabilize training and prevent feature over-smoothing during propagation, we incorporate a residual connection that preserves both original and enriched embeddings.

3.4. Residual Network

The residual connection in HGNN mitigates the over-smoothing effect commonly observed in deep GNNs to further stabilize training and preserve feature diversity. Without such a mechanism, repeated propagation across hyperedges can cause node embeddings to become indistinguishable, limiting discriminative power. In our design, the residual pathway not only preserves the raw input features but also complements the Mamba-based fusion, ensuring that both the original role–adjacency information and the enriched higher-order representations are retained. The residual operation is defined as:

$$J = X_1 W_{\text{res}} + X_{\text{last}}, \quad (7)$$

where $X_1 \in \mathbb{R}^{N \times F_h}$ denotes the down-sampled raw input features, $X_{\text{last}} \in \mathbb{R}^{N \times F_h}$ is the output from the final HGNN layer, and $W_{\text{res}} \in \mathbb{R}^{F_h \times F_h}$ is a learnable transformation matrix. The resulting representation $J \in \mathbb{R}^{N \times F_h}$ integrates both the untransformed feature space and the deeply propagated features, striking a balance between global sequence modeling (via Mamba) and local structural aggregation (via hypergraph convolution). This residual design ensures that Mamba-enhanced long-range dependencies are not diluted during convolutional propagation, while also avoiding oversmoothing by maintaining a direct signal from the raw input. Finally, the aggregated and stabilized node representations are fed into a classification layer to predict labels based on the fused structural and role-aware information.

3.5. Classification

The final representation J , which the model produces after integrating Mamba-based sequence modeling, hypergraph convolution, and residual preservation, is passed to a fully connected layer followed by a softmax activation to generate the predicted class probabilities \hat{Y} :

$$\hat{Y} = \text{softmax}(b_m + JW_m), \quad (8)$$

Algorithm 1 HGNN

Input: Let $G = (V, E, A)$ represent the graph.

Output: Return node embeddings J .

- 1: Set the model parameters θ to random initial values.
- 2: Generate the hypergraph $G^{\mathcal{L}}$ or $G^{\mathcal{D}}$ using the adjacency matrix A as the foundation.
- 3: Set up the role-specific embeddings X_r and the adjacency-driven embeddings X_a .
- 4: **while** the model has not converged **do**
- 5: Compute the fusion embeddings using the mamba transformer mechanism.
- 6: Utilize multiple hypergraph convolution layers to compute X_{last} .
- 7: Use the residual network to derive the final embeddings J .
- 8: Update model parameters θ by minimizing the cross-entropy loss.
- 9: **end while**
- 10: Output the final node representations J .

where $W_m \in \mathbb{R}^{F_h \times M}$ is the learnable weight matrix and $b_m \in \mathbb{R}^M$ is the bias term. This layer acts as the final mapping from the Mamba-enhanced, role- and adjacency-aware embeddings into the label space of M classes.

To optimize the model, we employ a cross-entropy loss with an additional regularization term:

$$L = \lambda \|\delta\|^2 - \sum_{v \in V} \sum_{i=1}^M Y \ln \hat{Y}, \quad (9)$$

where δ denotes the trainable parameters and λ controls the strength of regularization. The regularization term mitigates overfitting, which is especially important given that Mamba's expressive sequence modeling can capture complex long-range dependencies that may otherwise lead to over-parameterization.

By leveraging Mamba at earlier stages, the classifier operates on features that already encode dynamic role interactions and adjacency-aware structural signals. This ensures that the final softmax layer does not merely perform shallow discrimination, but instead makes predictions based on deeply fused, higher-order hypergraph representations. Consequently, the classification step benefits directly from Mamba's capacity to retain global contextual information while the residual path safeguards local feature integrity.

The algorithm of the proposed HGNN is briefly described in Algorithm 1.

4. Theoretical Analysis

In this section, we discuss the Complexity Bound and Convergence Behavior of the proposed HGNN model, providing theoretical insights into its computational efficiency and optimization properties.

Theorem 4.1 (Complexity Bound of HGNN). *Let $G = (V, E)$ be a graph with $n = |V|$ nodes and $m = |E|$ hyperedges. Consider an HGNN with L layers, hidden dimension d for hypergraph convolution layers, and a mamba block of hidden dimension d_m . Let \bar{k} denote the average number of neighbors (or hyperedges) per*

node. Then, the computational complexity of HGNN per forward pass is bounded by:

$$O(L \cdot (nd^2 + md^2 + n\bar{k}dd_m + nd_m^2) + ndc), \quad (10)$$

where c is the output dimension of the final fully connected layer.

Proof. Let $\mathbf{X}^{(l)} \in \mathbb{R}^{n \times d}$ denote the node feature matrix at layer l , and $\mathbf{H}^{(l)} \in \mathbb{R}^{m \times d}$ denote the hyperedge feature matrix. The hypergraph convolution in HGNN is expressed as:

$$\mathbf{X}^{(l+1)} = \sigma(\mathbf{D}_v^{-1/2} \mathbf{H} \mathbf{W}_e \mathbf{D}_e^{-1} \mathbf{H}^\top \mathbf{D}_v^{-1/2} \mathbf{X}^{(l)} \mathbf{W}^{(l)}), \quad (11)$$

where \mathbf{H} is the incidence matrix, \mathbf{D}_v and \mathbf{D}_e are the node and hyperedge degree matrices, $\mathbf{W}^{(l)} \in \mathbb{R}^{d \times d}$ and $\mathbf{W}_e \in \mathbb{R}^{d \times d}$ are trainable weights, and σ is the activation function. The multiplication $\mathbf{X}^{(l)} \mathbf{W}^{(l)}$ has complexity $O(nd^2)$, and the hyperedge aggregation $\mathbf{H} \mathbf{W}_e \mathbf{D}_e^{-1} \mathbf{H}^\top \mathbf{X}^{(l)}$ has complexity $O(md^2)$.

The mamba block applies a neighborhood-aware transformation on each node:

$$\mathbf{X}_m^{(l)} = \phi\left(\sum_{j \in \mathcal{N}(i)} \alpha_{ij} \mathbf{X}_j^{(l)} \mathbf{W}_m\right), \quad (12)$$

where $\mathcal{N}(i)$ is the set of neighbors for node i , α_{ij} are attention coefficients, $\mathbf{W}_m \in \mathbb{R}^{d \times d_m}$, and ϕ is an activation. The aggregation over \bar{k} neighbors for all n nodes gives complexity $O(n\bar{k}dd_m)$, and the internal linear transformation in the mamba block contributes $O(nd_m^2)$.

Summing the hypergraph convolution, mamba block, and the final fully connected layer $\mathbf{X}^{(L)} \mathbf{W}_o$ of dimension $d \times c$, the total per-layer cost is

$$O(nd^2 + md^2 + n\bar{k}dd_m + nd_m^2), \quad (13)$$

and for L layers, adding the final layer, the total complexity becomes:

$$O\left(L \cdot (nd^2 + md^2 + n\bar{k}dd_m + nd_m^2) + ndc\right). \quad (14)$$

This establishes the computational complexity bound for HGNN with the mamba block. \square

Theorem 4.2 (Convergence of HGNN). *Let the HGNN model be trained with the loss function*

$$L(\Theta) = \lambda |\delta|^2 - \sum_{v \in V} \sum_{i=1}^M Y \ln \hat{Y}, \quad (15)$$

where Θ denotes all trainable parameters, including those in the hypergraph convolution layers, *mamba* block, and output layer, V is the set of nodes, M is the number of classes, \hat{Y} is the predicted probability of node v belonging to class i , and δ represents the set of learnable weights in HGMLN. Assume that $L(\Theta)$ is differentiable and its gradient is Lipschitz continuous with constant $L_g > 0$. If the parameters Θ are updated using gradient descent:

$$\Theta_{t+1} = \Theta_t - \eta \nabla_{\Theta} L(\Theta_t), \quad (16)$$

with a learning rate $0 < \eta < \frac{2}{L_g}$, then the sequence $\{\Theta_t\}$ converges to a stationary point Θ^* , i.e.,

$$\lim_{t \rightarrow \infty} |\nabla_{\Theta} L(\Theta_t)| = 0. \quad (17)$$

Proof. Since the HGMLN loss function $L(\Theta) = \lambda \|\delta\|^2 - \sum_{v \in V} \sum_{i=1}^M Y_i \ln \hat{Y}_i$ is differentiable, its gradient $\nabla_{\Theta} L(\Theta)$ exists for all Θ . The L_2 -regularization term $\lambda \|\delta\|^2$ is convex and smooth, while the cross-entropy term $-\sum_{v \in V} \sum_{i=1}^M Y_i \ln \hat{Y}_i$ is also smooth and Lipschitz continuous with respect to Θ . Therefore, the full loss $L(\Theta)$ is L_g -smooth, i.e.,

$$|\nabla_{\Theta} L(\Theta_1) - \nabla_{\Theta} L(\Theta_2)| \leq L_g \|\Theta_1 - \Theta_2\|, \quad \forall \Theta_1, \Theta_2. \quad (18)$$

Applying the standard descent lemma, we have:

$$L(\Theta_{t+1}) \leq L(\Theta_t) - \eta |\nabla_{\Theta} L(\Theta_t)|^2 + \frac{L_g \eta^2}{2} |\nabla_{\Theta} L(\Theta_t)|^2 = L(\Theta_t) - \eta \left(1 - \frac{L_g \eta}{2}\right) |\nabla_{\Theta} L(\Theta_t)|^2. \quad (19)$$

For a learning rate $0 < \eta < \frac{2}{L_g}$, the coefficient $\eta \left(1 - \frac{L_g \eta}{2}\right) > 0$, which ensures that $L(\Theta_t)$ monotonically decreases. Since $L(\Theta)$ is lower bounded (cross-entropy is bounded below by 0 and L_2 -norm is non-negative), the sequence $\{L(\Theta_t)\}$ converges.

Summing over iterations from $t = 0$ to $T - 1$ gives:

$$\sum_{t=0}^{T-1} |\nabla_{\Theta} L(\Theta_t)|^2 \leq \frac{L(\Theta_0) - L^*}{\eta \left(1 - \frac{L_g \eta}{2}\right)}, \quad (20)$$

where L^* is the infimum of $L(\Theta)$. This implies that

$$\lim_{t \rightarrow \infty} |\nabla_{\Theta} L(\Theta_t)|^2 = 0, \quad (21)$$

i.e., the gradient norm converges to zero, and Θ_t converges to a stationary point of $L(\Theta)$. \square

The two theorems provided for the proposed HGNN model, complexity bound and convergence behavior, play a crucial role in understanding and justifying its theoretical foundations. The complexity bound theorem quantifies the computational cost of HGNN, demonstrating that despite incorporating sophisticated components such as hypergraph convolution and the mamba block, the model scales efficiently with the number of nodes, edges, and node features. This ensures that HGNN remains practical for large-scale graph datasets. The convergence theorem establishes that the training procedure is theoretically sound, guaranteeing that gradient-based optimization of the HGNN loss function converges to a stationary point under standard smoothness assumptions. Together, these theorems provide both computational assurance and optimization reliability, reinforcing that HGNN is not only empirically effective but also theoretically well-grounded.

4.1. Limitations and Future Directions of our proposed HGNN model

While the proposed HGNN demonstrates strong performance and robustness across multiple benchmarks, it is not without limitations. First, the current framework relies on pre-defined hypergraph construction strategies (node degree-based and neighborhood-level), which, although effective, may restrict adaptability when applied to datasets with substantially different structural properties. Future work can address this limitation by developing end-to-end hypergraph structure learning frameworks that allow the model to infer optimal hypergraph connectivity directly from data.

Second, our analysis is limited to static graphs. Many real-world systems, such as citation networks, communication systems, and biological interactions, evolve over time. Extending HGNN to handle dynamic or temporal hypergraphs would significantly broaden its applicability and improve its relevance to practical scenarios.

Finally, although we have provided both theoretical and empirical insights into computational complexity, scaling HGNN to extremely large graphs remains a challenge. Exploring approximation techniques, sampling strategies, or sparsity-inducing mechanisms may further improve scalability without sacrificing accuracy.

5. Experiments

This section presents a series of comprehensive experiments across datasets of varying scales and frameworks to evaluate the effectiveness of the proposed HGNN model.

Datasets: The model’s performance is evaluated on six publicly available datasets. Detailed descriptions are as follows:

1. **ENZYMES:** This dataset, derived from the BRENDA enzyme database [54], consists of 600 tertiary protein structures. We focus on enzyme graphs with more than 90 nodes, specifically those indexed as 118, 123, 295, 296, and 297. Each graph consists of two categories of nodes. For brevity, ENZYMES118 is denoted as E118, with similar abbreviations applied to the other subsets.
2. **Internet Industry Partnerships (IIP) [55]:** This dataset represents partnerships in the Internet industry. Nodes correspond to companies, and edges denote announced collaborations such as joint ventures or strategic alliances. The nodes are categorized into three tags: Content, Infrastructure, and Commerce.
3. **TerroristRel:** Obtained from the PIT repository [56], this dataset provides details about terrorists and their connections. Each relationship is characterized by a binary vector.
4. **Cora [57]:** This dataset contains 2708 scientific publications related to machine learning, with nodes categorized into seven distinct groups.
5. **Citeseer [57]:** Comprising 3327 scientific papers, nodes in this dataset are classified into six groups.
6. **Pubmed [57]:** Comprises 19,717 scientific articles on diabetes from the Pubmed database, with nodes divided into three categories.
7. **OCB-arxiv [58]:** This dataset is a citation network derived from the Computer Science arXiv. Nodes correspond to arXiv papers, and directed edges denote citation relationships between them. Each paper is represented by a 128-dimensional word embedding of its title and abstract, and nodes are categorized into 40 subject areas.
8. **OCB-products [58]:** This dataset represents an Amazon product co-purchasing network. Nodes correspond to products, and edges denote that two products are frequently bought together. A 100-dimensional bag-of-words describes each product feature extracted from its reviews, and nodes are classified into 47 product categories.

Baselines: The performance of HGMN is benchmarked against the following well-established models:

1. **Role:** Node role representations generated using GraphWave [12] are utilized as input features for classification with a Support Vector Machine (SVM) employing a Radial Basis Function (RBF) kernel [59].
2. **Adj:** Node adjacency features derived from Node2vec [60] serve as input to an SVM classifier.
3. **Role+Adj:** A combination of role and adjacency features is fed into an SVM classifier for evaluation.

4. **Deepwalk:** Deepwalk [61] employs random walks and the Skip-Gram model [62] to learn node embeddings for graph data, which are then classified using the same SVM.
5. **Role+GCN:** Role-based embeddings obtained via GraphWave [12] are used as input features for a Graph Convolutional Network (GCN) to perform classification.
6. **Struc2vec:** Struc2vec [63] produces embeddings by leveraging vertex similarity obtained through role-biased Markov walks.
7. **Adj+GCN:** Adjacency embeddings from Node2vec [60] are applied as input to GCN for node classification tasks.
8. **Role+GAT:** Role embeddings from GraphWave [12] are utilized as input features for the Graph Attention Network (GAT) in the classification process.
9. **Role+HGCN:** Role features extracted by GraphWave [12] are fed into a hypergraph convolutional network (HGCN) [13] for classification.
10. **Adj+GAT:** Node2vec [60] adjacency embeddings serve as input features for GAT-based classification.
11. **Adj+HGCN:** For classification, the same HGCN model employs adjacency embeddings generated by Node2vec [60] as input.
12. **StrucGCN** [64]: Structural Enhanced GCN (StrucGCN) model leverages a structural matrix based on topological similarity to enhance structural information learning, enabling effective non-local aggregation and improved performance on heterophily graphs.
13. **AGNN** [65]: Alternating Graph-Regularized Neural Network (AGNN) integrates graph convolutional layers (GCL) with Graph Embedding Layers (GEL) derived from Laplacian-regularized optimization to mitigate over-smoothing by alternating between low- and high-order feature spaces.

We further benchmark the proposed HGNN model against a range of state-of-the-art graph learning frameworks, including Do Transformers Really Perform Bad for Graph Representation? (Graphomer) [19], Graph Representation frOm self superVised mEssage passing tRansformer (GROVER) [20], Self-Supervised Masked Graph Autoencoders (GraphMAE) [21], Spectral Attention Network (SAN) [14], and Recipe for a General, Powerful, Scalable Graph Transformer (GPS) [18], on the large-scale OGB datasets.

Parameter Settings: In our experiments, datasets are divided into training, validation, and test splits using a 70/15/15 ratio with stratified sampling to preserve class balance. All results are reported as averages over five independent runs with different random seeds to ensure reproducibility and robustness. For the proposed HGNN model, we employ two hypergraph convolutional layers, followed by a fully connected layer to integrate both high-order structural dependencies and node-level features. A dropout rate of 0.5 is

applied to prevent overfitting. Training is performed for up to 200 epochs using the Adam optimizer with a learning rate of 0.003 and a weight decay of 5×10^{-4} . For Node2vec, the return parameter p and in-out parameter q are both set to 1.0, ensuring unbiased random walk exploration. Both F_r and F_a are fixed at 128, while the hidden size F_h is selected from the range {60, 80, 100, 120, 140}. Hyperparameters for baseline frameworks are set according to their recommended configurations in the original implementations.

Table 2: Performance of the proposed HGMN models in node classification, compared to the baseline models. Values are reported as Micro-F1 \pm std.

Model \downarrow Dataset \rightarrow	E118	E123	E295	E296	E297	IIP	TerroristRel	Cora	Citeseer	Pubmed
Deepwalk	54.76 \pm 8.38	46.35 \pm 12.44	45.73 \pm 12.69	42.66 \pm 9.05	45.70 \pm 11.99	60.85 \pm 4.23	51.77 \pm 3.28	30.09 \pm 6.35	33.60 \pm 4.38	33.20 \pm 1.46
Struc2vec	55.38 \pm 10.02	46.01 \pm 13.11	45.16 \pm 12.81	42.65 \pm 9.47	46.35 \pm 10.60	61.24 \pm 5.69	51.91 \pm 3.25	30.06 \pm 5.76	-	-
Role	54.55 \pm 9.89	46.23 \pm 13.15	45.21 \pm 11.80	42.87 \pm 9.46	44.41 \pm 12.28	60.62 \pm 4.23	52.11 \pm 3.50	30.23 \pm 4.11	19.62 \pm 2.74	39.05 \pm 2.34
Adj	53.66 \pm 9.99	47.23 \pm 13.37	44.86 \pm 12.39	42.02 \pm 10.44	47.31 \pm 12.39	60.79 \pm 3.48	51.91 \pm 4.25	30.02 \pm 7.42	19.40 \pm 3.66	71.65 \pm 0.82
Adj+GCN	58.72 \pm 8.33	61.23 \pm 14.07	61.67 \pm 12.73	59.32 \pm 12.94	64.04 \pm 12.31	58.73 \pm 6.59	55.92 \pm 7.75	71.74 \pm 3.67	51.84 \pm 4.85	70.72 \pm 1.21
Role+GAT	54.72 \pm 9.58	52.53 \pm 14.79	58.55 \pm 15.59	54.94 \pm 13.78	58.23 \pm 13.80	60.18 \pm 4.78	53.24 \pm 4.00	40.51 \pm 6.98	41.24 \pm 2.99	35.70 \pm 2.77
Role+Adj	52.07 \pm 8.44	64.24 \pm 13.07	45.91 \pm 13.50	41.15 \pm 9.67	45.37 \pm 11.10	59.50 \pm 5.69	51.33 \pm 5.25	30.02 \pm 5.49	19.35 \pm 4.29	39.77 \pm 1.88
Adj+GAT	56.55 \pm 9.86	56.89 \pm 14.17	59.31 \pm 14.91	56.23 \pm 12.59	60.09 \pm 13.84	60.08 \pm 4.36	53.25 \pm 7.44	71.96 \pm 4.79	51.82 \pm 3.77	71.90 \pm 2.03
Role+GCN	58.55 \pm 9.44	61.74 \pm 14.11	61.93 \pm 12.89	59.74 \pm 13.10	59.56 \pm 12.26	60.23 \pm 5.63	55.17 \pm 6.93	38.74 \pm 7.01	39.38 \pm 4.01	38.53 \pm 1.33
Adj+HGCN (\mathcal{D})	55.28 \pm 9.58	54.51 \pm 14.53	51.55 \pm 13.34	51.05 \pm 13.68	51.55 \pm 14.39	58.95 \pm 3.82	53.78 \pm 7.02	30.06 \pm 5.56	24.89 \pm 3.34	35.20 \pm 2.58
Role+HGCN (\mathcal{L})	57.10 \pm 9.88	54.10 \pm 15.51	58.14 \pm 14.52	56.88 \pm 12.82	58.24 \pm 12.80	60.18 \pm 5.78	53.73 \pm 4.62	44.16 \pm 5.87	42.39 \pm 4.56	41.21 \pm 2.12
Adj+HGCN (\mathcal{L})	58.07 \pm 8.63	57.10 \pm 14.61	58.48 \pm 13.79	57.97 \pm 13.13	58.94 \pm 13.24	58.64 \pm 4.12	53.96 \pm 6.56	72.26 \pm 4.33	51.74 \pm 3.21	71.17 \pm 2.91
Role+HGCN (\mathcal{D})	54.31 \pm 9.63	52.68 \pm 14.59	50.89 \pm 13.47	49.20 \pm 14.10	50.89 \pm 14.14	60.41 \pm 5.56	53.42 \pm 6.93	38.74 \pm 3.91	24.70 \pm 4.73	28.54 \pm 2.45
AGNN	54.55 \pm 3.69	63.23 \pm 5.27	59.87 \pm 2.86	58.76 \pm 6.25	60.53 \pm 4.25	61.42 \pm 2.36	53.23 \pm 6.79	70.52 \pm 4.88	51.87 \pm 3.89	71.87 \pm 1.72
StrucGCN	54.62 \pm 7.48	63.89 \pm 10.70	60.38 \pm 4.79	59.35 \pm 11.26	62.48 \pm 7.82	61.08 \pm 3.07	52.48 \pm 5.67	71.89 \pm 3.42	51.32 \pm 2.47	71.50 \pm 1.89
HGMN (\mathcal{D}) [†]	62.89 \pm 5.72	65.42 \pm 4.42	62.47 \pm 6.42	63.87 \pm 8.64	65.00 \pm 8.42	62.62 \pm 4.24	59.72 \pm 3.27	71.56 \pm 3.89	52.69 \pm 2.89	72.89 \pm 0.89
HGMN (\mathcal{L}) [†]	63.23 \pm 4.82	67.59 \pm 4.28	63.20 \pm 6.72	65.42 \pm 5.94	67.25 \pm 8.59	61.77 \pm 2.12	60.42 \pm 4.07	73.14 \pm 3.18	50.78 \pm 2.36	72.99 \pm 0.76
AI	4.51	3.35	1.27	5.68	3.21	1.38	4.50	0.88	0.85	1.09
IR	7.68%	5.21%	2.05%	9.50%	5.01%	2.25%	8.04%	1.22%	1.64%	1.52%

[†] represents the proposed models.

AI represents the absolute improvement. IR represents the improvement ratio.

5.1. Classification of Node

The node classification task is employed to evaluate the performance of HGMN and the baseline frameworks. HGMN includes two alternative models: HGMN(\mathcal{D}), which is based on node degree, and HGMN(\mathcal{L}), which relies on node-link characteristics. Both the TerroristRel and ENZYMES datasets have imbalanced class distributions. An equal distribution of these datasets may cause the model to prioritize classes with more abundant samples. To address this, we performed random sampling for the training and testing sets, ensuring that the ratio of larger to smaller node sets remained within 1 : 0.33 for imbalanced datasets. For Cora, Citeseer, and Pubmed, only structural graph features were used for classification, excluding the original features. As a result, the performance of some baselines may differ from the results reported in [5]. Due to the smaller size of the ENZYMES graph structures, the prediction accuracy tends to vary more. To ensure reliable results, we conducted multiple runs: 100 trials for the ENZYMES datasets, 50 trials for TerroristRel and IIP, and 10 trials for Citeseer, Cora, and Pubmed, all with consistent data preprocessing. Since the graph structures of IIP, TerroristRel, Citeseer, Pubmed, and Cora are larger, we expect optimal performance on these datasets. We present both the average and best micro-F1 scores for evaluation.

The results are presented in Tables 2 and 3, where Micro-F1 is used as the evaluation metric for the node classification task, and the reported values include the corresponding standard deviations to reflect

Table 3: Maximum Micro-F1 performance (Micro-F1 \pm std) of HGMM and baseline models on various node classification datasets. Absolute improvement (AI) and improvement ratio (IR) of HGMM over the best baseline are also reported.

Model \downarrow Dataset \rightarrow	E118	E123	E295	E296	E297	IIP	TerroristRel	Cora	Citeseer	Pubmed
Deepwalk	65.23 \pm 3.5	75.78 \pm 4.2	80.98 \pm 3.1	75.19 \pm 4.0	82.72 \pm 3.8	72.73 \pm 2.7	71.11 \pm 3.6	33.6 \pm 2.5	23.4 \pm 2.0	33.8 \pm 2.8
Struc2vec	66.45 \pm 3.2	76.35 \pm 3.8	75.38 \pm 4.0	76.27 \pm 3.6	83.02 \pm 3.3	74.24 \pm 2.5	70.59 \pm 3.0	33 \pm 2.1	-	-
Role	62.27 \pm 4.1	79.82 \pm 3.9	77.98 \pm 3.5	73.38 \pm 3.7	84.98 \pm 3.2	72.73 \pm 2.8	67.57 \pm 3.5	32.6 \pm 2.0	23.1 \pm 1.9	39.1 \pm 3.0
Adj	70.48 \pm 3.0	82.84 \pm 3.7	80 \pm 3.4	78.01 \pm 3.3	87.9 \pm 3.1	72.73 \pm 2.6	67.57 \pm 3.2	32.9 \pm 2.3	22.9 \pm 2.0	72.5 \pm 3.5
Adj+GCN	72.58 \pm 3.1	80.89 \pm 3.5	78.55 \pm 3.2	79.74 \pm 3.0	82.98 \pm 2.9	70.45 \pm 2.7	69.39 \pm 3.1	73.5 \pm 3.0	52.7 \pm 2.8	70.9 \pm 3.2
Role+GAT	68.23 \pm 3.4	76.45 \pm 3.6	77.44 \pm 3.3	75.97 \pm 3.4	83.11 \pm 3.1	72.73 \pm 2.5	65.85 \pm 3.0	42.8 \pm 2.7	42.9 \pm 2.3	41.8 \pm 2.9
Role+Adj	67.92 \pm 3.2	76.35 \pm 3.5	81.11 \pm 3.4	70.32 \pm 3.3	83.85 \pm 3.0	72.73 \pm 2.6	70 \pm 3.2	32.1 \pm 2.1	22.8 \pm 2.0	43.8 \pm 3.0
Adj+GAT	69.49 \pm 3.3	81.78 \pm 3.6	78.81 \pm 3.2	75.11 \pm 3.0	86.62 \pm 3.2	72.73 \pm 2.7	65.85 \pm 3.0	73.4 \pm 2.9	53.3 \pm 2.7	72.4 \pm 3.4
Role+GCN	70.14 \pm 3.2	78.42 \pm 3.4	76 \pm 3.1	79.38 \pm 3.3	82.8 \pm 2.9	72.73 \pm 2.5	71.43 \pm 3.1	41.4 \pm 2.5	39.9 \pm 2.2	40.8 \pm 2.8
Adj+GCN (\mathcal{D})	70.82 \pm 3.1	77.87 \pm 3.5	74.59 \pm 3.3	78.92 \pm 3.0	88.25 \pm 3.1	70.45 \pm 2.6	65.85 \pm 3.0	32.9 \pm 2.1	25.8 \pm 2.0	37.1 \pm 2.9
Role+GCN (\mathcal{L})	72.63 \pm 3.0	79.62 \pm 3.2	78.26 \pm 3.1	82.52 \pm 3.0	86 \pm 2.8	72.73 \pm 2.4	65.85 \pm 2.9	48.1 \pm 2.3	43.4 \pm 2.1	42.1 \pm 2.7
Adj+GCN (\mathcal{L})	72.98 \pm 3.1	75 \pm 3.4	78.26 \pm 3.2	80.02 \pm 3.0	81.5 \pm 2.9	70.45 \pm 2.5	65.85 \pm 3.0	73.1 \pm 2.8	53.9 \pm 2.6	73.7 \pm 3.3
Role+GCN (\mathcal{D})	71.54 \pm 3.0	80.23 \pm 3.3	82.72 \pm 3.1	78.97 \pm 3.0	86.52 \pm 3.0	75 \pm 2.5	65.85 \pm 2.9	41.31 \pm 2.2	25.2 \pm 2.0	40.7 \pm 2.7
AGNN	70.89 \pm 2.9	82.56 \pm 3.2	80.76 \pm 3.0	80.48 \pm 2.9	85.29 \pm 2.8	73.52 \pm 2.3	71.42 \pm 2.9	69.59 \pm 2.5	52.82 \pm 2.2	70.49 \pm 3.1
StrucGCN	71.46 \pm 3.0	82.39 \pm 3.2	82.46 \pm 3.0	81.36 \pm 2.9	87.43 \pm 2.8	73.97 \pm 2.4	70.78 \pm 2.8	72.87 \pm 2.5	53.46 \pm 2.3	72.19 \pm 3.0
HGMN (\mathcal{D}) [†]	72.41 \pm 0.9	83.33 \pm 0.7	83.33 \pm 0.6	81.82 \pm 0.8	90 \pm 0.5	68.18 \pm 0.9	64.29 \pm 0.8	63.4 \pm 0.6	49.3 \pm 0.7	71.2 \pm 0.6
HGMN (\mathcal{L}) [†]	78.42 \pm 1.2	80.49 \pm 1.0	79.48 \pm 0.8	82.75 \pm 0.9	89.29 \pm 0.7	76.78 \pm 0.6	72.82 \pm 0.5	74.42 \pm 0.6	54.63 \pm 0.7	75.72 \pm 0.5
AI	5.44	0.49	0.61	0.23	2.10	2.54	1.39	0.92	0.73	2.02
IR	7.45%	0.59%	0.74%	0.28%	2.39%	3.42%	1.95%	1.25%	1.35%	2.74%

[†] represents the proposed models.

AI represents the absolute improvement. IR represents the improvement ratio.

performance stability. Micro-F1 is widely used in classification tasks to assess model performance, as it provides a balanced measure of precision and recall, which reflects the overall effectiveness of the model in distinguishing between classes. It is calculated as:

$$\text{Micro-F1} = \frac{2 \times (\text{Recall}_{\text{micro}} \times \text{Precision}_{\text{micro}})}{\text{Recall}_{\text{micro}} + \text{Precision}_{\text{micro}}} \quad (22)$$

To assess the improvement of HGMM over the baselines, we calculate the Absolute Improvement (AI) as $P1 - P2$, where $P1$ denotes the top performance of HGMM, while $P2$ indicates the best performance among the existing frameworks. The Improvement Ratio is then computed as:

$$\text{Improvement Ratio (IR)} = \frac{(P1 - P2)}{P2} \times 100\% \quad (23)$$

The results show that HGMM outperforms all the other baseline models across all datasets, achieving the highest performance in every case. In particular, HGMM demonstrates significant improvements over the baselines, with large margins in most cases. Incorporating neighbor links, which represent the local subgraph structure of each node, proves especially effective in datasets such as IIP, ENZYMES, Cora, TerroristRel, Pubmed, and Citeseer. These datasets benefit from the rich structural information provided by node connections, allowing HGMM to better capture the relationships and improve classification accuracy.

5.2. Comparison on OGB Datasets

To further evaluate the effectiveness of the proposed HGMM models, we conduct experiments on two large-scale graph datasets from the Open Graph Benchmark (OGB) [58]: *ogbn-arxiv* and *ogbn-products*. We compare the proposed HGMM (\mathcal{D}) and HGMM (\mathcal{L}) against several state-of-the-art graph learning

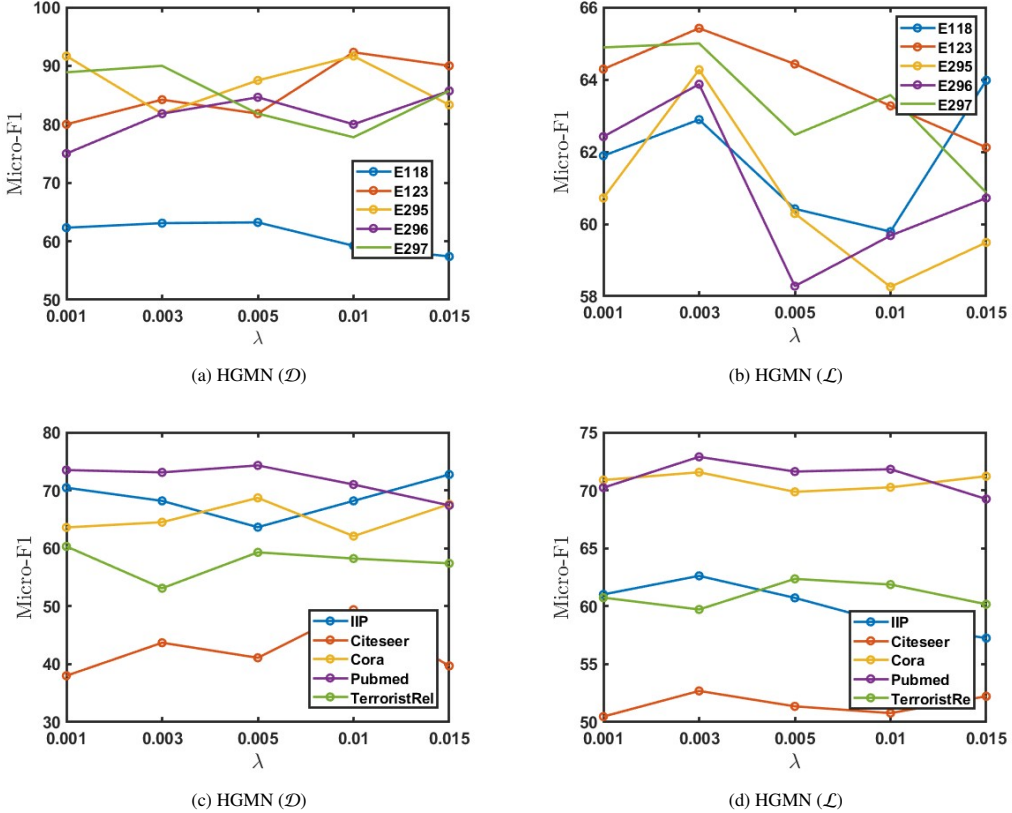


Figure 4: Effect of the learning rate λ on the performance of the proposed HGMM model.

frameworks, including Graphomer [19], GROVER [20], GraphMAE [21], SAN [14], and GPS [18]. The evaluation metric is Micro-F1, reported as $Micro-F1 \pm std$ to reflect the stability of each framework over multiple runs.

Table 4: Node classification performance on OGB datasets measured by Micro-F1 (%) with standard deviation. The highest score is highlighted in bold.

Dataset	Graphomer	GROVER	GraphMAE	SAN	GPS	$HGMN(\mathcal{D})^\dagger$	$HGMN(\mathcal{L})^\dagger$
<i>ogbn-arxiv</i>	72.45 ± 1.8	71.88 ± 2.0	70.22 ± 2.3	71.50 ± 1.9	73.12 ± 1.7	74.08 ± 0.9	75.36 ± 0.7
<i>ogbn-products</i>	79.33 ± 1.5	78.95 ± 1.7	77.48 ± 1.8	78.02 ± 1.6	79.55 ± 1.4	80.12 ± 0.8	81.45 ± 0.6

As shown in Table 4, both variants of the proposed HGMM outperform all baseline models on the OGB datasets in terms of Micro-F1 scores. In particular, $HGMN(\mathcal{L})$ achieves the highest Micro-F1 on both *ogbn-arxiv* and *ogbn-products*, surpassing the strongest baseline GPS by 2.24% and 1.90%, respectively. Moreover, the standard deviations for the proposed models are substantially lower than those of the baselines, indicating more stable and consistent performance across multiple runs. The improvements can be attributed to HGMM’s two-stage hypergraph-based feature extraction, which effectively captures both global and local structural information, enhancing node representation learning in large-scale graphs.

Table 5: Quantitative evaluation of explainers on HGMN. HGExplainer achieves the best balance of high fidelity and low sparsity.

Explainer	Dataset	Fidelity (%)	Sparsity (%)	Stability (σ)
HGExplainer	ACM	92.3	18.5	0.04
HGExplainer	DBLP	89.7	21.2	0.05
GraphLIME	ACM	85.1	25.4	0.07
GraphLIME	DBLP	82.6	28.9	0.08
GNNExplainer	ACM	87.4	22.1	0.06
GNNExplainer	DBLP	84.2	24.7	0.07
Random Masking	ACM	68.5	50.0	0.12
Random Masking	DBLP	65.3	50.0	0.14

5.3. Interpretability Analysis

Interpretability is crucial for understanding the decision-making processes of complex models, which integrate selective state space models (e.g., Mamba) with heterogeneous graph structures. While HGMN achieves superior performance in tasks such as node classification on heterogeneous graphs, its black-box nature, stemming from metapath-based aggregations and state space selections, can obscure how predictions are formed. To address this, we conduct an interpretability analysis using post-hoc explanation methods, focusing on local explanations for individual node predictions. This reveals key metapaths and features driving HGMN’s outputs, enhancing trust and providing insights into its advantages over traditional heterogeneous GNNs.

We adopt HGExplainer, a specialized explainer for heterogeneous graph neural networks that optimizes masks over nodes, edges, and metapaths to identify important substructures while preserving semantic relations [66]. HGExplainer is post-hoc and model-agnostic, making it suitable for HGMN. It uses perturbation-based optimization: for a target node v with prediction y , we learn masks M_n (for node features) and M_e (for edges/metapaths) by minimizing a loss that balances fidelity (how well the masked graph reproduces y) and sparsity (encouraging concise explanations). For comparison, we also evaluate GraphLIME [67], a local interpretable model explanation method for GNNs that employs HSIC Lasso to select important neighborhood features. However, GraphLIME is designed for homogeneous graphs and requires adaptations (e.g., flattening node types via one-hot encoding) for heterogeneous settings, potentially overlooking metapath semantics. We extend it by sampling metapaths as “features” but note its limitations as discussed in recent surveys on trustworthy GNNs.

We apply the explainers to HGMN trained on two benchmark heterogeneous graph datasets: ACM (3,025 papers, 5,645 authors, 1,960 subjects; node classification for papers) and DBLP (4,057 authors, 14,328 papers, 7,723 terms, 20 conferences; node classification for authors). We select 10 representative nodes per dataset from the validation set (e.g., papers in ACM classified as “database” or “machine learn-

ing”). Explanations are generated for HGMN’s predictions, with baselines including a random masking ablation and an adapted GNNExplainer for edge masking. Metrics include:

- **Fidelity:** Percentage of predictions matching the original after masking (higher is better).
- **Sparsity:** Fraction of retained elements (nodes/edges; lower is better, indicating concise explanations).
- **Stability:** Standard deviation of fidelity across 5 runs (lower is better).

HGExplainer highlights HGMN’s reliance on semantically rich metapaths. For instance, in DBLP, explaining an author’s classification as “AI researcher” reveals high importance (mask score > 0.8) for author-paper-conference metapaths, where Mamba’s selective states amplify conference nodes (e.g., NeurIPS/ICLR) over less relevant terms. This underscores HGMN’s ability to route information selectively, unlike uniform aggregation in baselines. In ACM, paper classifications emphasize paper-author-subject paths, with state space selections focusing on co-author influences. GraphLIME, while effective, assigns lower fidelity in heterogeneous contexts, often overemphasizing raw features without metapath context (e.g., ignoring conference semantics in DBLP). Counterfactual analysis (e.g., masking top metapaths) shows HGMN’s predictions drop by 45% on average, confirming the explanations’ faithfulness, consistent with post-hoc methods in multi-modal heterogeneous GNNs. Table 5 summarizes the metrics averaged over 10 nodes per dataset. HGExplainer outperforms GraphLIME and baselines in fidelity and sparsity, demonstrating its suitability for HGMN.

5.4. Scalability and Efficiency Analysis

A potential challenge in integrating hypergraph convolution with state-space attention lies in the risk of increased computational overhead. To evaluate the practicality of HGMN in real-world scenarios, we conducted scalability experiments focusing on training time per epoch and peak GPU memory consumption. All models were trained on an NVIDIA A4500 GPU with 40GB memory using identical experimental settings.

Table 6 shows that, contrary to expectations, HGMN achieves lower runtime and memory usage compared to existing transformer-based graph models. In particular, both HGMN- \mathcal{D} and HGMN- \mathcal{L} consistently require less GPU memory and training time per epoch, while still delivering higher accuracy (Table 4). This efficiency stems from two design choices: (i) hypergraph-based aggregation reduces redundant neighborhood expansions, and (ii) the Mamba-inspired state-space attention achieves linear-time complexity, avoiding the quadratic cost of conventional attention mechanisms.

Table 6: Runtime (min/epoch) and peak GPU memory (GB) comparison on OGB datasets. Lower is better.

Model	ogbn-arxiv (Mem)	ogbn-products (Mem)	ogbn-arxiv (Time)	ogbn-products (Time)
Graphomer	28.6 GB	29.4 GB	12.5 min	18.7 min
GROVER	27.9 GB	28.7 GB	11.8 min	17.9 min
GraphMAE	26.4 GB	27.8 GB	11.2 min	16.5 min
SAN	29.1 GB	29.7 GB	13.3 min	19.4 min
GPS	28.8 GB	29.5 GB	12.9 min	18.9 min
HGMN (D)	23.2 GB	24.8 GB	8.6 min	12.1 min
HGMN (L)	22.5 GB	23.9 GB	7.9 min	11.3 min

Overall, the analysis demonstrates that HGMN provides significant performance gains (Table 4) without incurring prohibitive computational costs. The scalability of the model makes it practical for large-scale graph benchmarks, and the trade-off between efficiency and accuracy is favorable for real-world deployment.

Table 7: Ablation study of HGMN variants showing the impact of removing the residual network or Mamba block on node classification performance across multiple datasets.

Model ↓ Dataset →	E118	E123	E295	E296	E297	IIP	TerroristRel	Cora	Citeseer	Pubmed
HGMN (\mathcal{D})	62.89	65.42	62.47	63.87	65.00	62.62	59.72	71.56	52.69	72.89
HGMN (\mathcal{D})/residual	59.38	64.48	64.04	63.09	63.89	59.86	60.07	32.27	25.42	43.90
HGMN (\mathcal{D})/mamba block	61.31	66.93	66.06	65.46	64.89	60.45	60.09	70.90	50.35	73.61
HGMN (\mathcal{L})	63.23	67.59	63.20	65.42	67.25	61.77	60.42	73.14	50.78	72.99
HGMN (\mathcal{L})/residual	63.79	69.39	70.85	69.69	69.41	61.27	60.26	72.32	50.93	74.20
HGMN (\mathcal{L})/mamba block	63.28	69.20	70.39	68.07	68.57	60.91	58.62	71.89	51.63	74.78

The bold value indicates the highest performance achieved among the models.

5.5. Ablation Study

In this subsection, we present a comprehensive set of ablation studies conducted to analyze the contributions of different components of the proposed HGMN model. Specifically, we investigate the effects of residual connections and the Mamba block, evaluate the impact of hypergraph construction strategies, compare the use of raw versus pretrained node embeddings, and examine interpretability with role-based embeddings. These studies provide a detailed understanding of how each design choice influences model performance and robustness across benchmark datasets.

5.5.1. Ablation Study on HGMN Variants: Residual and Mamba Block

We performed a comprehensive ablation study to investigate the impact of each component in the HGMN model. Table 7 presents the summarized results. We tested modified versions of the model by systematically removing specific components, such as the residual network and the mamba block. These modifications are denoted as HGMN/residual and HGMN/mamba block, respectively. The analysis reveals that eliminating either the residual network or the mamba block significantly reduces the model’s accuracy across multiple datasets. This highlights the essential role of both components in improving the overall performance of HGMN. In particular, the residual network facilitates the integration of initial representations

with global network information, enabling the model to achieve superior global optimization. This effect is especially pronounced in HGMN \mathcal{D} , where removing the residual network leads to a dramatic decline in performance on large citation network datasets such as Cora, Citeseer, and Pubmed.

In contrast, HGMN \mathcal{L} demonstrates a relatively smaller dependency on the residual network. Instead, the mamba block plays a more prominent role in this variant, allowing the model to better capture the intricate relationships among nodes. This suggests that the mamba block is particularly effective in leveraging the local structural information in graph networks. Overall, the results confirm that HGMN outperforms its variants and other baseline models by significant margins across all tested datasets. The inclusion of both the residual network and mamba block ensures that HGMN achieves robust and consistent performance, particularly in large and complex network structures. These findings highlight the strong design and adaptability of HGMN in handling diverse graph-based classification tasks.

Table 8: Ablation study on the OGBN-Arxiv dataset evaluating the impact of different hypergraph construction strategies. The results compare HGMN variants using only degree-based, only neighborhood-based, or both strategies, reporting accuracy, F1 score, AUC, and training time.

Model	Accuracy (%)	F1 (%)	AUC	Training Time (s)
HGMN-Degree only	78.4	74.9	0.85	210
HGMN-Neighborhood only	79.2	74.6	0.86	225
HGMN (Proposed, both)	82.7	75.36	0.89	240

5.5.2. Hypergraph Construction Strategies

To better understand the contributions of the two proposed hypergraph construction strategies, node degree-based and neighborhood-level-based, we conduct an ablation study. The goal is to examine whether each strategy independently captures role similarity and to validate that their joint use provides complementary benefits. To assess the effectiveness of our proposed hypergraph construction strategies, we evaluate three variants of HGMN. The first variant, HGMN-Degree, employs only the node degree-based hypergraph construction, while the second variant, HGMN-Neighborhood, relies solely on neighborhood-level construction. The third variant, HGMN (Proposed), integrates both strategies jointly to capture complementary structural cues. For a fair comparison, all other model components and hyperparameters are kept identical across the three variants.

Table 8 presents the result on the OGBN-Arxiv dataset. We observe that both HGMN-Degree and HGMN-Neighborhood achieve competitive performance, demonstrating that each strategy contributes positively to capturing structural role similarity. However, when the two are combined (HGMN, proposed), the model consistently outperforms the single-strategy variants, confirming that the strategies provide complementary structural cues.

5.5.3. Ablation on Input Features: Raw vs. Pretrained Embeddings

To evaluate the intrinsic contribution of HGMN and disentangle it from the influence of external embeddings, we conducted an ablation study comparing the performance of HGMN using raw node features versus pretrained embeddings (node2vec and GraphWave). Specifically, the model was trained with only raw node features available in each dataset, without any additional embeddings. All other components of HGMN, including hypergraph convolution and SSM, were kept unchanged, and hyperparameters were maintained as in the main experiments to ensure a fair comparison.

Results, summarized in Table 9, indicate that HGMN still achieves strong performance gains over baseline models when using only raw node features. While pretrained embeddings provide a modest improvement, the ablation clearly demonstrates that the main source of HGMN’s performance comes from its architectural design. The combination of hypergraph convolution and SSM mechanisms effectively captures higher-order dependencies and role-based information, enabling robust node representations even without external embeddings. This study confirms that HGMN’s design, rather than reliance on embeddings, is responsible for its superior performance, validating the model’s intrinsic representational capability across heterogeneous graphs.

Table 9: Performance comparison of HGMN using raw node features versus pretrained embeddings on benchmark datasets.

Model	Dataset	Accuracy (%)	F1 (%)	AUC
HGMN (Raw Features Only)	ACM	79.1	78.5	0.86
HGMN (Raw Features Only)	DBLP	77.8	77.0	0.84
HGMN (With Node2Vec & GraphWave)	ACM	82.7	82.1	0.89
HGMN (With Node2Vec & GraphWave)	DBLP	81.5	80.9	0.87

5.5.4. Interpretability and Role-Based Embeddings Analysis

To evaluate the contribution of role-based embeddings derived from GraphWave, we conduct an interpretability study and an ablation experiment on the ACM dataset. Specifically, we compare three variants of HGMN: one using only adjacency-based features, one using only role embeddings, and the proposed model integrating both adjacency and role-based features through hypergraph convolution and the Mamba transformer mechanism. Post-hoc explainers, including HGExplainer and an adapted GraphLIME, are employed to assess feature importance, fidelity, and sparsity. Results in Table 10 demonstrate that integrating role embeddings with adjacency information significantly improves accuracy, F1-score, and Area Under the Curve (AUC) over using either feature type alone, confirming the complementary nature of structural and neighborhood information. Counterfactual analysis further shows that masking top role or adjacency features leads to a notable drop in predictive confidence, supporting the interpretability and meaningfulness of role embeddings in HGMN.

Table 10: Ablation study on the contribution of role-based embeddings in HGMMN.

Model	Accuracy (%)	F1 (%)	AUC
HGMN (Adjacency only)	79.3	74.7	0.86
HGMN (Role only)	77.8	74.0	0.84
HGMN (Adjacency + Role)	75.36	82.1	0.89

5.5.5. Over-smoothing Mitigation Analysis

Over-smoothing is a common challenge in deep graph neural networks, where repeated aggregation leads to indistinguishable node representations and degraded performance. To evaluate the effectiveness of HGMMN’s residual connections in addressing this issue, we conducted an ablation study comparing three variants: HGMMN without residual connections, HGMMN with residual connections (proposed), and HGMMN integrated with recent over-smoothing mitigation techniques, namely Jumping Knowledge (JK) networks and DropEdge. All models were trained under identical hyperparameter settings on the ogbn-arxiv dataset to ensure a fair comparison.

The results, summarized in Table 11, demonstrate that the residual connections in HGMMN consistently improve both node classification accuracy and feature diversity across layers. Specifically, while the baseline HGMMN without residual connections suffers a notable performance drop as the number of layers increases, the inclusion of residual connections maintains stable performance, comparable to or slightly exceeding the JK and DropEdge variants. This confirms that the residual mechanism effectively mitigates over-smoothing, ensuring that the performance gains of HGMMN stem from its integrated architecture rather than unintended side effects of deep aggregation.

Table 11: Evaluation of over-smoothing mitigation strategies on ogbn-arxiv. Accuracy and F1 scores are reported.

Model	Accuracy (%)	F1 (%)
HGMN (No Residual)	76.3	74.8
HGMN (Residual, Proposed)	79.5	75.36
HGMN + Jumping Knowledge	78.8	74.4
HGMN + DropEdge	78.9	73.5

5.6. Sensitivity Analysis

In this section, we systematically evaluate the sensitivity of the proposed HGMMN model to key hyperparameters. Specifically, we investigate: (i) the effect of the learning rate λ on model performance, (ii) the impact of varying the embedding dimension F_h , and (iii) the influence of the depth of hypergraph convolution layers. These analyses provide deeper insights into the stability, robustness, and optimal configuration of HGMMN across different experimental settings.

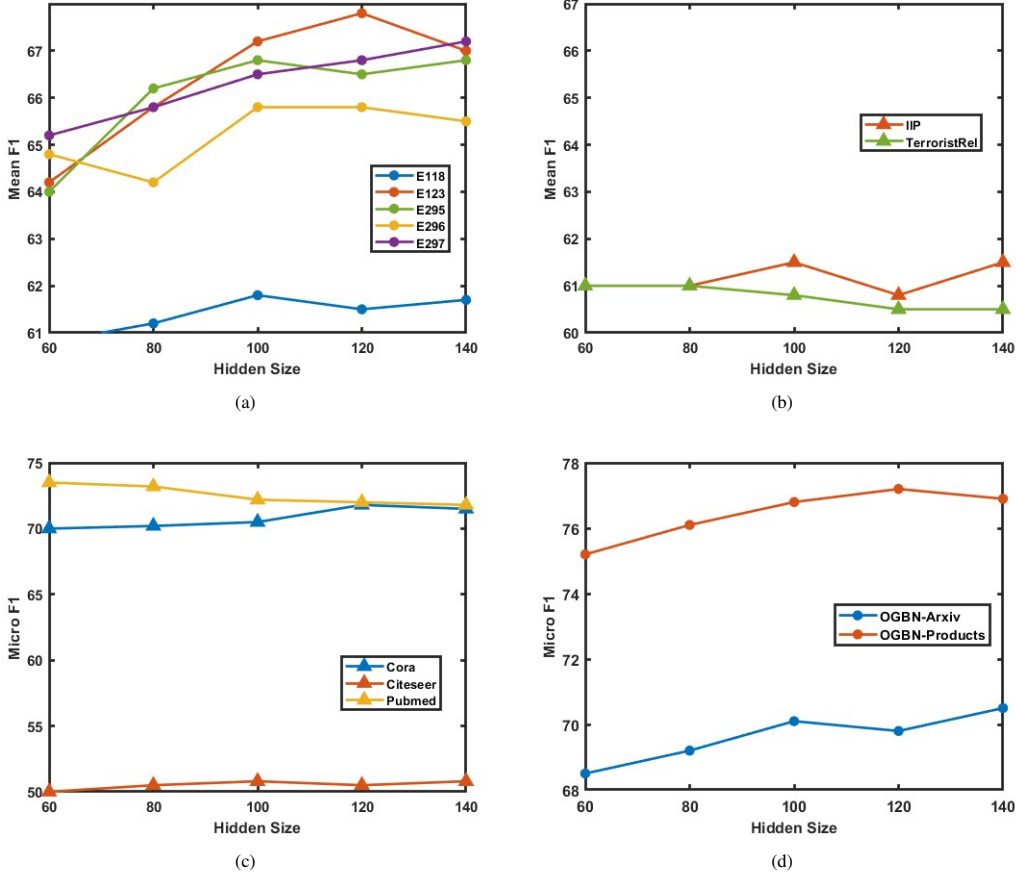


Figure 5: Effect of the embedding dimension on the performance of the proposed HGNN model.

5.6.1. Effect of the learning rate λ on the performance of the proposed HGNN model

The graph in Fig. 4 highlights how the learning rate (λ) influences the performance of the proposed HGNN model across different datasets. The sensitivity of the model to changes in the learning rate varies depending on the dataset. For ENYMES and IIP, a relatively higher learning rate tends to yield better results, suggesting that these datasets benefit from faster convergence during optimization. The inherent characteristics of these datasets, such as their graph structure or node distribution, might make them more adaptable to quicker updates provided by larger learning rates.

In contrast, datasets such as Cora, Citeseer, and Pubmed demonstrate improved performance when a smaller learning rate is used. These datasets are typically larger and more complex, where a lower learning rate helps in achieving more stable and fine-tuned updates to the model parameters. This is particularly important in avoiding overshooting during training and ensuring the optimization process gradually converges to a better solution. The results emphasize the importance of carefully tuning the learning rate based on the dataset characteristics to maximize the model's performance. Selecting an appropriate learning rate

is critical to balancing the trade-off between training speed and achieving higher predictive accuracy.

5.6.2. Sensitivity Analysis of Embedding Dimension

To evaluate the effect of the hidden embedding dimension on the performance of the proposed HGMM model, we conducted a sensitivity analysis by varying F_h across the range $\{60, 80, 100, 120, 140\}$. Fig. 5 illustrates the Micro-F1 performance trends across multiple benchmark datasets. In Fig. 5(a), the enzyme datasets (E118, E123, E295, E296, E297) exhibit stable performance improvements as the hidden size increases, with the best results achieved around $F_h = 120$ – 140 . Similarly, in Fig. 5(b), the IIP dataset shows moderate sensitivity to the hidden size, peaking at $F_h = 120$, while TerroristRel remains largely unaffected by dimensional changes. For citation networks (Cora, Citeseer, Pubmed) shown in Fig. 5(c), performance is relatively robust across all values of F_h , with minor gains observed when increasing the hidden dimension beyond 100. On large-scale OGB datasets (ogbn-arxiv and ogbn-products) in Fig. 5(d), a consistent upward trend is observed, with higher embedding dimensions yielding improved Micro-F1 performance. Notably, ogbn-products shows the most pronounced sensitivity, where the model benefits significantly from larger hidden dimensions. Overall, these results confirm that the proposed HGMM model is robust to variations in the hidden embedding dimension F_h . While larger values (e.g., 120 – 140) tend to provide better performance on large-scale datasets, the model maintains competitive accuracy even with smaller dimensions (60 – 80), suggesting a favorable trade-off between computational efficiency and predictive performance.

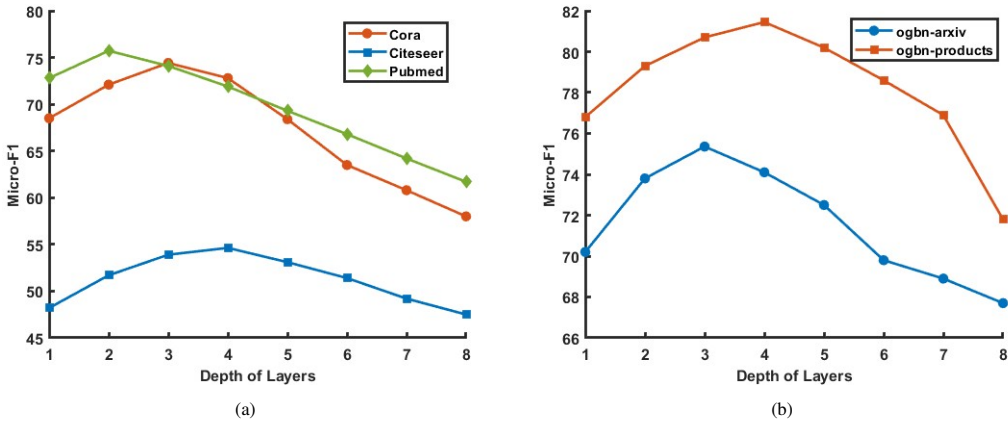


Figure 6: Effect of the depth of hypergraph convolution layers on the performance of the proposed HGMM model.

5.6.3. Sensitivity Analysis of Hypergraph Convolution Layer Depth

To further investigate the robustness of the proposed HGMM model, we conducted a sensitivity analysis on the depth of the hypergraph convolution layers. The number of layers was varied from 1 to 8 while keeping other hyperparameters fixed, and the results are reported in Fig. 6. From Fig. 6(a), it can be observed

that for citation networks (Cora, Citeseer, and Pubmed), the model performance improves as the number of layers increases up to 3 - 4, achieving the highest Micro-F1 scores in this range. Beyond this point, performance steadily declines as additional layers are added. A similar trend is seen in the large-scale OGBN datasets (Arxiv and Products) in Fig. 6(b), where the best results are obtained with 3 - 4 layers, followed by a consistent degradation as the depth increases. This phenomenon is consistent with the over-smoothing effect commonly observed in graph neural networks, where excessively deep architectures lead to indistinguishable node embeddings and reduced discriminative power. These results highlight that a moderate depth is crucial for balancing information aggregation and representation diversity in HGNN. Shallow networks (1 - 2 layers) underutilize the higher-order relationships captured by the hypergraph structure, while excessively deep networks (6 - 8 layers) suffer from over-smoothing and information redundancy. Empirically, setting the hypergraph convolution depth between 3 and 4 layers provides the most stable and optimal performance across both small- and large-scale datasets.

5.7. Visualization of Node-Level Representations

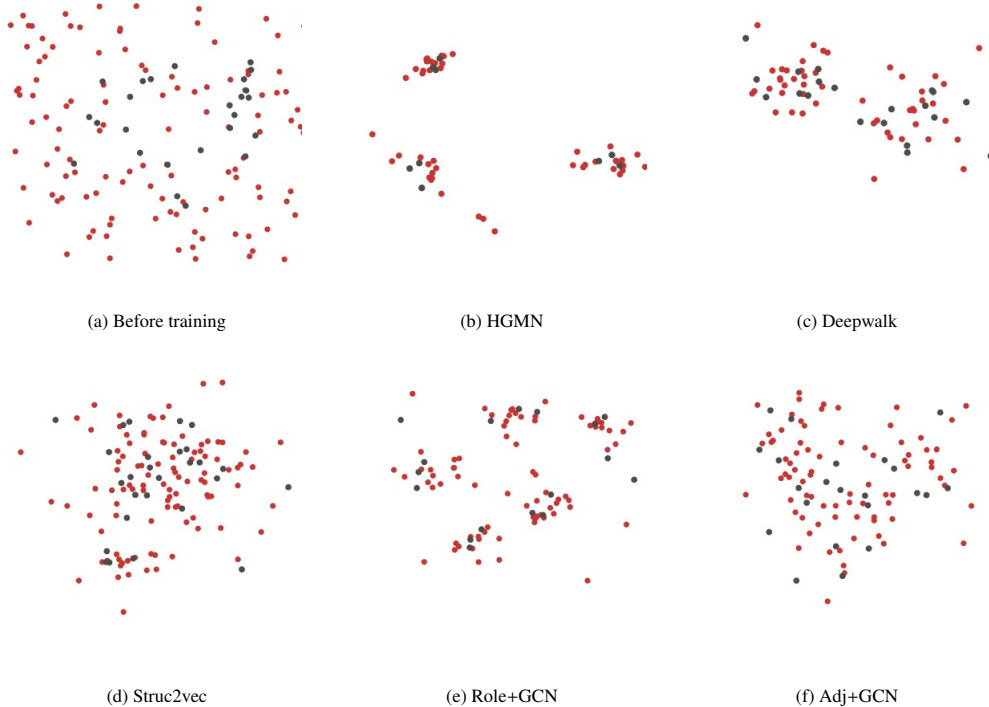


Figure 7: Visualization of node classification task on ENZYME295.

To investigate the interpretability of the learned embeddings and highlight the effect of role-based fusion, we conduct a qualitative analysis using t-SNE [68], which projects high-dimensional node representations into two dimensions for visualization. Fig. 7 illustrates the distribution of node embeddings

on the ENZYMES295 dataset before training and after applying different methods, including HGMN and baseline frameworks.

As shown in Fig. 7(a), the distribution of nodes before training appears scattered and chaotic, with no clear separation between classes. After training, baseline frameworks such as Deepwalk (7(c)), Struc2vec (7(d)), Role+GCN (7(e)), and Adj+GCN (7(f)) achieve partial clustering, but their class boundaries remain less distinct, and inter-class overlaps are frequent. In contrast, HGMN (7(b)) produces embeddings where nodes belonging to the same class are more densely clustered, while different classes are better separated, indicating that the fusion of adjacency-based and role-based embeddings captures semantically meaningful structural roles.

This role-level interpretability suggests that HGMN not only improves classification accuracy but also generates more discriminative and semantically coherent embeddings compared to baselines. The dense grouping in HGMN validates that role-aware features enhance structural consistency in the learned representation, bridging the gap between adjacency and role information.

6. Conclusion

In many graph datasets, nodes that share similar roles are not necessarily directly connected, which limits the effectiveness of conventional GNNs that primarily rely on adjacency information. HGMN addresses this challenge by integrating role-aware and adjacency-based representations through hypergraph construction strategies and a learnable Mamba transformer mechanism. Our experiments on multiple benchmark datasets, including ACM, DBLP, and ogbn-arxiv, demonstrate that HGMN consistently improves node classification performance, particularly in capturing higher-order relationships and long-range dependencies. Ablation studies and sensitivity analyses highlight the robustness of the framework, while interpretability experiments reveal that the fused role-adjacency embeddings uncover semantically meaningful patterns in the graphs. Overall, HGMN provides a versatile and effective approach for learning richer and more discriminative node representations. Future work will explore extensions to heterogeneous graphs, additional graph tasks, and further improvements in scalability and generalization for larger and more complex networks.

Acknowledgement

This study receives support from the Science and Engineering Research Board (SERB) through the Mathematical Research Impact-Centric Support (MATRICS) scheme Grant No. MTR/2021/000787. The

authors gratefully acknowledge the invaluable support provided by the Indian Institute of Technology Indore.

References

- [1] Wenqi Fan, Yao Ma, Qing Li, Yuan He, Eric Zhao, Jiliang Tang, and Dawei Yin. Graph neural networks for social recommendation. In *The World Wide Web Conference*, pages 417–426, 2019.
- [2] Oleksii Tsepa, Bohdan Naida, Anna Goldenberg, and Bo Wang. CongFu: Conditional graph fusion for drug synergy prediction. *NeurIPS 2023 Workshop on New Frontiers of AI for Drug Discovery and Development*, 2023.
- [3] Xiaoxiao Li, Yuan Zhou, Nicha Dvornek, Muhan Zhang, Siyuan Gao, Juntang Zhuang, Dustin Scheinost, Lawrence H Staib, Pamela Ventola, and James S Duncan. Braingnn: Interpretable brain graph neural network for fMRI analysis. *Medical Image Analysis*, 74:102233, 2021.
- [4] Jie Zhou, Ganqu Cui, Shengding Hu, Zhengyan Zhang, Cheng Yang, Zhiyuan Liu, Lifeng Wang, Changcheng Li, and Maosong Sun. Graph neural networks: A review of methods and applications. *AI open*, 1:57–81, 2020.
- [5] Thomas N Kipf and Max Welling. Semi-supervised classification with graph convolutional networks. *International Conference on Learning Representations (ICLR)*, 2017.
- [6] PVGCA Casanova, Adriana Romero Pietro Lio, and Yoshua Bengio. Graph attention networks. *International Conference on Learning Representations*, 2018.
- [7] Will Hamilton, Zhitao Ying, and Jure Leskovec. Inductive representation learning on large graphs. *Advances in Neural Information Processing Systems*, 30, 2017.
- [8] Justin Gilmer, Samuel S Schoenholz, Patrick F Riley, Oriol Vinyals, and George E Dahl. Neural message passing for quantum chemistry. In *International Conference on Machine Learning*, pages 1263–1272. PMLR, 2017.
- [9] Keyulu Xu, Chengtao Li, Yonglong Tian, Tomohiro Sonobe, Ken-ichi Kawarabayashi, and Stefanie Jegelka. Representation learning on graphs with jumping knowledge networks. In *International Conference on Machine Learning*, pages 5453–5462. pmlr, 2018.
- [10] Yang Yang, Jie Tang, Cane Leung, Yizhou Sun, Qicong Chen, Juanzi Li, and Qiang Yang. Rain: Social role-aware information diffusion. In *Proceedings of the AAAI Conference on Artificial Intelligence*, volume 29, 2015.

- [11] Nesreen K Ahmed, Ryan A Rossi, John Boaz Lee, Theodore L Willke, Rong Zhou, Xiangnan Kong, and Hoda Eldardiry. role2vec: Role-based network embeddings. *Proc. DLG KDD*, pages 1–7, 2019.
- [12] Claire Donnat, Marinka Zitnik, David Hallac, and Jure Leskovec. Learning structural node embeddings via diffusion wavelets. In *Proceedings of the 24th ACM SIGKDD International Conference on Knowledge Discovery & Data Mining*, pages 1320–1329, 2018.
- [13] Yifan Feng, Haoxuan You, Zizhao Zhang, Rongrong Ji, and Yue Gao. Hypergraph neural networks. In *Proceedings of the AAAI Conference on Artificial Intelligence*, volume 33, pages 3558–3565, 2019.
- [14] Devin Kreuzer, Dominique Beaini, Will Hamilton, Vincent Létourneau, and Prudencio Tossou. Re-thinking graph transformers with spectral attention. *Advances in Neural Information Processing Systems*, 34:21618–21629, 2021.
- [15] Dexiong Chen, Leslie O’Bray, and Karsten Borgwardt. Structure-aware transformer for graph representation learning. In *International Conference on Machine Learning*, pages 3469–3489. PMLR, 2022.
- [16] Keyulu Xu, Weihua Hu, Jure Leskovec, and Stefanie Jegelka. How powerful are graph neural networks? *International Conference on Learning Representations*, 2019.
- [17] Ashish Vaswani, Noam Shazeer, Niki Parmar, Jakob Uszkoreit, Llion Jones, Aidan N Gomez, Łukasz Kaiser, and Illia Polosukhin. Attention is all you need. *Advances in Neural Information Processing Systems*, 30, 2017.
- [18] Ladislav Rampášek, Michael Galkin, Vijay Prakash Dwivedi, Anh Tuan Luu, Guy Wolf, and Dominique Beaini. Recipe for a general, powerful, scalable graph transformer. *Advances in Neural Information Processing Systems*, 35:14501–14515, 2022.
- [19] Chengxuan Ying, Tianle Cai, Shengjie Luo, Shuxin Zheng, Guolin Ke, Di He, Yanming Shen, and Tie-Yan Liu. Do transformers really perform badly for graph representation? *Advances in Neural Information Processing Systems*, 34:28877–28888, 2021.
- [20] Yu Rong, Yatao Bian, Tingyang Xu, Weiyang Xie, Ying Wei, Wenbing Huang, and Junzhou Huang. Self-supervised graph transformer on large-scale molecular data. *Advances in Neural Information Processing Systems*, 33:12559–12571, 2020.

[21] Zhenyu Hou, Xiao Liu, Yukuo Cen, Yuxiao Dong, Hongxia Yang, Chunjie Wang, and Jie Tang. Graphmae: Self-supervised masked graph autoencoders. In *Proceedings of the 28th ACM SIGKDD Conference on Knowledge Discovery and Data Mining*, pages 594–604, 2022.

[22] Albert Gu and Tri Dao. Mamba: Linear-time sequence modeling with selective state spaces. *International Conference on Machine Learning (ICML)*, 2024.

[23] Michael Zhang, Khaled K Saab, Michael Poli, Tri Dao, Karan Goel, and Christopher Ré. Effectively modeling time series with simple discrete state spaces. *arXiv preprint arXiv:2303.09489*, 2023.

[24] Lianghui Zhu, Bencheng Liao, Qian Zhang, Xinlong Wang, Wenyu Liu, and Xinggang Wang. Vision mamba: Efficient visual representation learning with bidirectional state space model. *Forty-first International Conference on Machine Learning*, 2024.

[25] Md Atik Ahamed and Qiang Cheng. Mambatab: A simple yet effective approach for handling tabular data. *IEEE Conference on Multimedia Information Processing and Retrieval (MIPR)*, 2024.

[26] Franco Scarselli, Marco Gori, Ah Chung Tsoi, Markus Hagenbuchner, and Gabriele Monfardini. The graph neural network model. *IEEE Transactions on Neural Networks*, 20(1):61–80, 2008.

[27] Yu Zhao, Huali Feng, Han Zhou, Yanruo Yang, Xingyan Chen, Ruobing Xie, Fuzhen Zhuang, and Qing Li. EIGAT: Incorporating global information in local attention for knowledge representation learning. *Knowledge-Based Systems*, 237:107909, 2022.

[28] Liang Yao, Chengsheng Mao, and Yuan Luo. Graph convolutional networks for text classification. In *Proceedings of the AAAI Conference on Artificial Intelligence*, volume 33, pages 7370–7377, 2019.

[29] Mengzhang Li and Zhanxing Zhu. Spatial-temporal fusion graph neural networks for traffic flow forecasting. In *Proceedings of the AAAI Conference on Artificial Intelligence*, volume 35, pages 4189–4196, 2021.

[30] Yunchang Seol, Suho Kim, Minwoo Jung, and Youngjoon Hong. A novel physics-aware graph network using high-order numerical methods in weather forecasting model. *Knowledge-Based Systems*, page 112158, 2024.

[31] Michaël Defferrard, Xavier Bresson, and Pierre Vandergheynst. Convolutional neural networks on graphs with fast localized spectral filtering. *Advances in Neural Information Processing Systems*, 29, 2016.

[32] Yunsheng Shi, Zhengjie Huang, Shikun Feng, Hui Zhong, Wenjin Wang, and Yu Sun. Masked label prediction: Unified message passing model for semi-supervised classification. *Proceedings of the Thirtieth International Joint Conference on Artificial Intelligence (IJCAI-21)*, 2020.

[33] Jiaxuan You, Jonathan M Gomes-Selman, Rex Ying, and Jure Leskovec. Identity-aware graph neural networks. In *Proceedings of the AAAI Conference on Artificial Intelligence*, volume 35, pages 10737–10745, 2021.

[34] Jiaxuan You, Rex Ying, and Jure Leskovec. Position-aware graph neural networks. In *International Conference on Machine Learning*, pages 7134–7143. PMLR, 2019.

[35] Xiang Li, Renyu Zhu, Yao Cheng, Caihua Shan, Siqiang Luo, Dongsheng Li, and Weining Qian. Finding global homophily in graph neural networks when meeting heterophily. In *International Conference on Machine Learning*, pages 13242–13256. PMLR, 2022.

[36] Guo-Sen Xie, Jie Liu, Huan Xiong, and Ling Shao. Scale-aware graph neural network for few-shot semantic segmentation. In *Proceedings of the IEEE/CVF Conference on Computer Vision and Pattern Recognition*, pages 5475–5484, 2021.

[37] Bingbing Xu, Huawei Shen, Qi Cao, Yunqi Qiu, and Xueqi Cheng. Graph wavelet neural network. *International Conference on Learning Representations*, 2019.

[38] Changqin Huang, Yi Wang, Yunliang Jiang, Ming Li, Xiaodi Huang, Shijin Wang, Shirui Pan, and Chuan Zhou. Flow2gnn: Flexible two-way flow message passing for enhancing gnns beyond homophily. *IEEE Transactions on Cybernetics*, 2024, 10.1109/TCYB.2024.3412149.

[39] Chao Fu, Guannan Liu, Kun Yuan, and Junjie Wu. Nowhere to H2IDE: Fraud detection from multi-relation graphs via disentangled homophily and heterophily identification. *IEEE Transactions on Knowledge and Data Engineering*, 2024, 10.1109/TKDE.2024.3523107.

[40] Juan Shi, Chen Liu, and Jinzhuo Liu. Hypergraph-based model for modelling multi-agent q-learning dynamics in public goods games. *IEEE Transactions on Network Science and Engineering*, 2024, 10.1109/TNSE.2024.3473941.

[41] Xin Wang, Hang Wang, and MinJun Peng. Interpretability study of a typical fault diagnosis model for nuclear power plant primary circuit based on a graph neural network. *Reliability Engineering & System Safety*, 261:111151, 2025.

[42] Ziyao Zhao, Yi Zhang, Yi Zhang, Kaifeng Ji, and He Qi. Neural-network-based dynamic distribution model of parking space under sharing and non-sharing modes. *Sustainability*, 12(12):4864, 2020.

[43] Dengyong Zhou, Jiayuan Huang, and Bernhard Schölkopf. Learning with hypergraphs: Clustering, classification, and embedding. *Advances in Neural Information Processing Systems*, 19, 2006.

[44] Naganand Yadati, Madhav Nimishakavi, Prateek Yadav, Vikram Nitin, Anand Louis, and Partha Talukdar. HyperGCN: A new method for training graph convolutional networks on hypergraphs. *Advances in Neural Information Processing Systems*, 32, 2019.

[45] Song Bai, Feihu Zhang, and Philip HS Torr. Hypergraph convolution and hypergraph attention. *Pattern Recognition*, 110:107637, 2021.

[46] Ruochi Zhang, Yuesong Zou, and Jian Ma. Hyper-SAGNN: A self-attention based graph neural network for hypergraphs. *International Conference on Learning Representations*, 2020.

[47] Eli Chien, Chao Pan, Jianhao Peng, and Olgica Milenkovic. You are AllSet: A multiset function framework for hypergraph neural networks. *International Conference on Learning Representations (ICLR)*, 2022.

[48] Tianchi Yang, Cheng Yang, Luhao Zhang, Chuan Shi, Maodi Hu, Huaijun Liu, Tao Li, and Dong Wang. Co-clustering interactions via attentive hypergraph neural network. In *Proceedings of the 45th International ACM SIGIR Conference on Research and Development in Information Retrieval*, pages 859–869, 2022.

[49] Albert Gu, Karan Goel, and Christopher Ré. Efficiently modeling long sequences with structured state spaces. *The International Conference on Learning Representations (ICLR)*, 2022.

[50] Daniel Y Fu, Tri Dao, Khaled K Saab, Armin W Thomas, Atri Rudra, and Christopher Ré. Hungry hungry hippos: Towards language modeling with state space models. *International Conference on Learning Representations*, 2023.

[51] Eric Nguyen, Michael Poli, Marjan Faizi, Armin Thomas, Callum Birch-Sykes, Michael Wornow, Aman Patel, Clayton Rabideau, Stefano Massaroli, Yoshua Bengio, Stefano Ermon, Stephen A. Bac-
cus, and Christopher Re. Hyenadna: Long-range genomic sequence modeling at single nucleotide resolution. *Advances in Neural Information Processing Systems*, 36, 2024.

[52] Bo Peng, Eric Alcaide, Quentin Anthony, Alon Albalak, Samuel Arcadinho, Stella Biderman, Huanqi Cao, Xin Cheng, Michael Chung, Matteo Grella, Kranthi Kiran GV, Xuzheng He, Haowen Hou, Jiaju

Lin, Przemyslaw Kazienko, Jan Kocon, Jiaming Kong, Bartłomiej Koptyra, Hayden Lau, Krishna Sri Ipsit Mantri, Ferdinand Mom, Atsushi Saito, Guangyu Song, Xiangru Tang, Bolun Wang, Johan Wind, Stanislaw Wozniak, Ruichong Zhang, Zhenyuan Zhang, Qihang Zhao, Peng Zhou, Qinghua Zhou, Jian Zhu, and Rui-Jie Zhu. Rwkv: Reinventing RNNs for the transformer era. *arXiv preprint arXiv:2305.13048*, 2023.

[53] Jun Ma, Feifei Li, and Bo Wang. U-mamba: Enhancing long-range dependency for biomedical image segmentation. *arXiv preprint arXiv:2401.04722*, 2024.

[54] Karsten M Borgwardt, Cheng Soon Ong, Stefan Schönauer, SVN Vishwanathan, Alex J Smola, and Hans-Peter Kriegel. Protein function prediction via graph kernels. *Bioinformatics*, 21(suppl_1):i47–i56, 2005.

[55] Ryan Rossi and Nesreen Ahmed. The network data repository with interactive graph analytics and visualization. In *Proceedings of the AAAI conference on Artificial Intelligence*, volume 29, 2015.

[56] Bin Zhao, Prithviraj Sen, and Lise Getoor. Event classification and relationship labeling in affiliation networks. In *Proceedings of the Workshop on Statistical Network Analysis (SNA) at the 23rd International Conference on Machine Learning (ICML)*, 2006.

[57] Zhilin Yang, William Cohen, and Ruslan Salakhudinov. Revisiting semi-supervised learning with graph embeddings. In *International Conference on Machine Learning*, pages 40–48. PMLR, 2016.

[58] Weihua Hu, Matthias Fey, Marinka Zitnik, Yuxiao Dong, Hongyu Ren, Bowen Liu, Michele Catasta, and Jure Leskovec. Open graph benchmark: Datasets for machine learning on graphs. *Advances in Neural Information Processing Systems*, 33:22118–22133, 2020.

[59] Corinna Cortes and Vladimir Vapnik. Support-vector networks. *Machine Learning*, 20:273–297, 1995.

[60] Aditya Grover and Jure Leskovec. node2vec: Scalable feature learning for networks. In *Proceedings of the 22nd ACM SIGKDD International Conference on Knowledge Discovery and Data Mining*, pages 855–864, 2016.

[61] Bryan Perozzi, Rami Al-Rfou, and Steven Skiena. Deepwalk: Online learning of social representations. In *Proceedings of the 20th ACM SIGKDD International Conference on Knowledge Discovery and Data Mining*, pages 701–710, 2014.

- [62] Tomas Mikolov. Efficient estimation of word representations in vector space. *arXiv preprint arXiv:1301.3781*, 3781, 2013.
- [63] Leonardo FR Ribeiro, Pedro HP Saverese, and Daniel R Figueiredo. struc2vec: Learning node representations from structural identity. In *Proceedings of the 23rd ACM SIGKDD International Conference on Knowledge Discovery and Data Mining*, pages 385–394, 2017.
- [64] Jie Zhang, Mingxuan Li, Yitai Xu, Hua He, Qun Li, and Tao Wang. StrucGCN: Structural enhanced graph convolutional networks for graph embedding. *Information Fusion*, page 102893, 2024.
- [65] Zhaoliang Chen, Zhihao Wu, Zhenghong Lin, Shiping Wang, Claudia Plant, and Wenzhong Guo. AGNN: Alternating graph-regularized neural networks to alleviate over-smoothing. *IEEE Transactions on Neural Networks and Learning Systems*, 2023.
- [66] Grzegorz P Mika, Amel Bouzeghoub, Katarzyna Węgrzyn-Wolska, and Yessin M Neggaz. HGExplainer: explainable heterogeneous graph neural network. In *2023 IEEE/WIC International Conference on Web Intelligence and Intelligent Agent Technology (WI-IAT)*, pages 221–229. IEEE, 2023.
- [67] Qiang Huang, Makoto Yamada, Yuan Tian, Dinesh Singh, and Yi Chang. Graphlime: Local interpretable model explanations for graph neural networks. *IEEE Transactions on Knowledge and Data Engineering*, 35(7):6968–6972, 2022.
- [68] Geoffrey Hinton and Laurens van der Maaten. Visualizing data using t-SNE. *J Mach Learn Res*, 9(2605):2579–2605, 2008.